

ABSTRACT

Thesis: MULTI-HAZARD OF A BRIDGE PIER DUE
TO EARTHQUAKE AND SCOUR

Hsiao-Chi Chen, Master of Science
Civil Engineering, 2008

Thesis Directed by: Professor Peter Chang
Department of Civil Engineering

Bridge structures are often subjected to multi-hazardous conditions, such as earthquake loading, scouring of the foundation, wind, flood, vehicle impact, etc. In the past, these hazards were considered as independent events that occur separately. Scouring, however, is a continuous phenomenon, therefore, bridges subjected to dynamic motion from earthquakes or vehicle impacts are also subjected to scouring simultaneously. When the scouring action is combined with dynamic motion, the result may be a synergistic action that the scour depth could be greater than the scour depth of considering these two damage factors occur sequentially. This paper is a preliminary study to investigate the possible synergistic effects of these combined hazards in experimental way.

MULTI-HAZARD OF A BRIDGE PIER DUE TO
EARTHQUAKE AND SCOUR

By
Hsiao-Chi Chen

Thesis submitted to the Faculty of the Graduate School of the
University of Maryland, College Park in partial fulfillment
Of the requirements for the degree of
Master of Science
2008

Advisory Committee:

Professor Peter Chang
Professor Sherif M. Aggour
Professor David Lovell

©Copyright by

University of Maryland

2008

Table of Contents

List of Tables	iv
List of Figures	vii
1. Introduction.....	1
1.1 Background.....	1
1.2 Scour Concept overview.....	2
1.3 Research Goals.....	4
2. Literature Review.....	6
2.1 The Flow Field at Piers Causing Local Scour.....	6
2.2 3-D Numerical Model of Scour around Circular Piers	7
2.3 Methods for Predicting Slope Displacements Induced by Earthquake.....	10
3. Scour with Harmonic Shaking Experiment.....	14
3.1 Experimental Setup.....	14
3.2 Experiment Procedure.....	20
3.3 Result Observations.....	23
3.4 Result Discussion.....	31
4. Scour with Simulated Earthquake Experiment.....	44
4.1 Experiment Setup.....	44

4.2 Experiment Procedure.....	47
4.3 Result Observations.....	51
4.4 Result Discussion.....	59
6. Conclusion.....	67
7. References.....	70

List of Tables

Table 3.1 coordinates of points at which the depths are measured.....	19
Table 3.2 the combination of shaking frequencies and flow rates used for experiments.....	23
Table 3.3 the depth readings of test <i>24cm/s7hz</i>	23
Table 3.4 the depth readings of test <i>24cm/s8hz</i>	24
Table 3.5 the depth readings of test <i>24cm/s9hz</i>	24
Table 3.6 the depth readings of test <i>25cm/s7hz</i>	25
Table 3.7 the depth readings of test <i>25cm/s8hz</i>	25
Table 3.8 the depth readings of test <i>25cm/s9hz</i>	26
Table 3.9 the depth readings of test <i>26cm/s7hz</i>	26
Table 3.10 the depth readings of test <i>26cm/s8hz</i>	27
Table 3.11 the depth readings of test <i>26cm/s9hz</i>	27
Table 3.12 the depth readings of test <i>27cm/s7hz</i>	28
Table 3.13 the depth readings of test <i>27cm/s8hz</i>	28
Table 3.14 the depth readings of test <i>27cm/s9hz</i>	29
Table 3.15 the depth readings of test <i>28cm/s7hz</i>	29
Table 3.16 the depth readings of test <i>28cm/s8hz</i>	30
Table 3.17 the depth readings of test <i>28cm/s9hz</i>	30

Table 3.18 the root mean square of the scour depths differences among superimposed tests and concurrent tests performed at different flow rates and different shaking frequencies.....	38
Table 3.19 the maximum scour depths (d/b) of the sequential tests and the concurrent tests.....	40
Table 3.20 the percent error of maximum scour depths of superimposed tests vs. concurrent tests (%).....	41
Table 3.21 the scouring volumes (cm ³) of the superimposed tests and the concurrent tests.....	42
Table 3.22 the percent error of the scouring volumes of superimposed tests vs. concurrent tests (%).....	42
Table 3.23 the cross-correlation coefficients of the sequential test and the concurrent test in harmonic shaking experiment.....	44
Table 4.1 the root mean squares of the differences between superimposed tests and concurrent tests	44
Table 4.2 the root mean squares of the differences between scour after superimposed tests and scour after concurrent tests.....	44
Table 4.3 the percent errors of the maximum scour depths of superimposed tests vs. concurrent tests	45

Table 4.4 the percent errors of the maximum scour depths of scouring after sequential tests vs. scouring after concurrent tests66

Table 4.5 the cross-correlation coefficients of the superimposed tests versus the concurrent tests in different flow rates66

Table 4.6 the cross-correlation coefficients of the scouring after superimposed tests versus the scouring after concurrent tests with different flow rates.66

List of Figures

Figure 1.1 the types of scour that can occur at a bridge.....	4
Figure 2.1 the flow and scour patterns at a circular pier.....	7
Figure 2.2 Comparison of simulated and experimental results of the scour depth evolution at the pier nose.....	9
Figure 2.3 Comparison of measured and simulated final bed elevation contours.....	9
Figure 2.4 Application of simplified sliding block method for the stability analysis of slopes. For $k > k_c$, sliding takes place on plane AB inclined to the horizontal by an angle β	11
Figure 3.1 the shaking flume.....	15
Figure 3.2 shaking streambed and pier.....	15
Figure 3.3 the robot arm and positioning motor for the harmonic shaking experiment.....	16
Figure 3.4 the laser displacement sensor for the harmonic shaking experiment	17
Figure 3.5 laser measurement sensor positioning.....	18
Figure 3.6 the surface of the streambed before and after a scouring experiment.....	19

Figure 3.7 the location of points around the pier where the depths are measured.....19

Figure 3.8 scatter plots of the scour depths of the superimposed test (3rd) versus concurrent test (6th) with flow rate of 24cm/s and specified harmonic shaking frequencies: (a) 7Hz (b) 8Hz (c) 9Hz.....33

Figure 3.9 scatter plots of the scour depths of the superimposed test (3rd) versus concurrent test (6th) with flow rate of 25cm/s and specified harmonic shaking frequencies: (a) 7Hz (b) 8Hz (c) 9Hz.....34

Figure 3.10 scatter plots of the scour depths of the superimposed test (3rd) versus concurrent test (6th) with flow rate of 26cm/s and specified harmonic shaking frequencies: (a) 7Hz (b) 8Hz (c) 9Hz.....35

Figure 3.11 scatter plots of the scour depths of the superimposed test (3rd) versus concurrent test (6th) with flow rate of 27cm/s and specified harmonic shaking frequencies: (a) 7Hz (b) 8Hz (c) 9Hz.....36

Figure 3.12 scatter plots of the scour depths of the superimposed test (3rd) versus concurrent test (6th) with flow rate of 28cm/s and specified harmonic shaking frequencies: (a) 7Hz (b) 8Hz (c) 9Hz.....37

Figure 4.1 the robot arm and positioning motor for the earthquake simulation experiment.....45

Figure 4.2 the picture of the laser displacement sensor for the simulated earthquake shaking experiment.....	46
Figure 4.3 the locations of the measured points in simulated earthquake shaking experiment.....	47
Figure 4.4 Labview program to simulate earthquake motions	48
Figure 4.5 the frequencies of the simulated earthquake	49
Figure 4.6 Mesh plot of scour surface for 25cm/s flow rate test.....	52
Figure 4.7 Mesh plot of scour surface for 26cm/s flow rate test.....	53
Figure 4.8 Mesh plot of scour surface for 27cm/s flow rate test.....	54
Figure 4.9 Mesh plot of scour surface for 28cm/s flow rate test.....	55
Figure 4.10(a) the contour plot of the superimposed test with 25cm/s flow rate. (b) the contour plot of the concurrent test with 25cm/s flow rate..	56
Figure 4.11(a) the contour plot of the superimposed test with 26cm/s flow rate. (b) the contour plot of the concurrent test with 26cm/s flow rate..	57
Figure 4.12(a) the contour plot of the superimposed test with 27cm/s flow rate. (b) the contour plot of the concurrent test with 27cm/s flow rate..	57
Figure 4.13(a) the contour plot of the scouring after superimposed test with 27cm/s flow rate. (b) the contour plot of the scouring after	

concurrent test with 27cm/s flow rate.....	58
Figure 4.14(a) the contour plot of the superimposed test with 28cm/s flow rate.	
(b) the contour plot of the concurrent test with 28cm/s flow rate..	58
Figure 4.15(a) the contour plot of the scouring after superimposed test with	
28cm/s flow rate. (b) the contour plot of the scouring after	
concurrent test with 28cm/s flow rate.....	59
Figure 4.16 Scatter plot of the scour depths of the superimposed test versus	
concurrent test with flow rate of 25cm/s for the simulated	
earthquake experiment.....	60
Figure 4.17 Scatter plot of the scour depths of the superimposed test versus	
concurrent test with flow rate of 26cm/s for the simulated	
earthquake experiment.....	61
Figure 4.18 Scatter plot of the scour depths of the superimposed test versus	
concurrent test with flow rate of 27cm/s for the simulated	
earthquake experiment.....	61
Figure 4.19 Scatter plot of the scour depths of the sequential test versus	
concurrent test with flow rate of 28cm/s for the simulated	
earthquake experiment.....	62
Figure 4.20 Scatter plot of the scour depths of the sequential test after scouring	

versus concurrent test after scouring with flow rate of 27cm/s for
the simulated earthquake experiment.....63

Figure 4.21 Scatter plot of the scour depths of the sequential test after scouring

versus concurrent test after scouring with flow rate of 28cm/s for
the simulated earthquake experiment.....63

INTRODUCTION

1.1 Background

Scour is the result of the erosive action of flowing water, carrying away material from bed and banks of streams and other waterways. When scour occurs on bridge structures, scour may erode the foundations of the bridges, ultimately leading to structural failure. The vertical and lateral changes in channel dimensions resulting from scour can jeopardize the bridge foundations and safety.

When the scouring is combined with the motion of shaking which may be due to earthquake loading, vehicle impact, or traffic induced vibration, the resulting effect may be a synergistic combination of the damage from scour and shaking, which maybe different from the superposition of the individual effects if they are considered independently. Seismic forces may weaken the compactness of the soil and make the scour condition worse or even activates a potential scour.

In the past, investigating the effect of both scour and shaking to the bridge, if considered, are often done by taking each one as separate and independent events. Nevertheless, in most condition, scour and earthquake or traffic induced vibration often happen concurrently. Understanding the results of these effects occurring sequentially and concurrently, however, is difficult, because the

equipment necessary to produce these effects concurrently did not exist.

In order to verify the possible synergy between scour and shaking, the Federal Highway Administration (FHWA) designed and installed a shaking flume at the Turner-Fairbank Highway Research Center (TFHRC). The shaking flume at TFHRC provides the first facility to experimentally observe these events concurrently. Using this experimental setup, the combined effects of scouring and earthquake motion on a bridge pier can now be simulated.

1.2 Scouring Concept Overview

Scour is caused by sediment carried away by flowing water. If sediment on which bridge supports rest is scoured by a river, the bridge could become unsafe for travel. In 1987, the Interstate Highway Bridge over Schoharie Creek in New York State collapsed during a flood. After the accident, the Federal Highway Administration required every State to identify highway bridges which are likely to have scour problems.

The types of scour affecting bridges can be categorized into three types:

1. General Scour: General scour is the long-term stream bed elevation changes due to natural causes or due to development of the river, its flood plain or watershed. This general sediment removal and resultant lowering of the

riverbed level is a natural process, but may remove large amounts of sediment over time.

2. Contraction Scour: Contraction scour involves the removal of material from the bed and banks across all or most of the channel width. Contraction scour is typically caused by an increase in speed of water as it moves through a bridge opening that is narrower than the natural river channel.

3. Local scour: Local scour involves the removal of material from around piers and abutments. Water flowing past a pier or abutment may scoop out holes in the sediment; these holes are known as scour holes. Local scour is caused by acceleration of flow and the resulting vortices induced by the flow obstructions.

The three different types of scour occurring at bridge are demonstrated in Figure 1.1 (Bruce W. M. and Stephen E. C., 2000). In this study, we will focus on local scour.

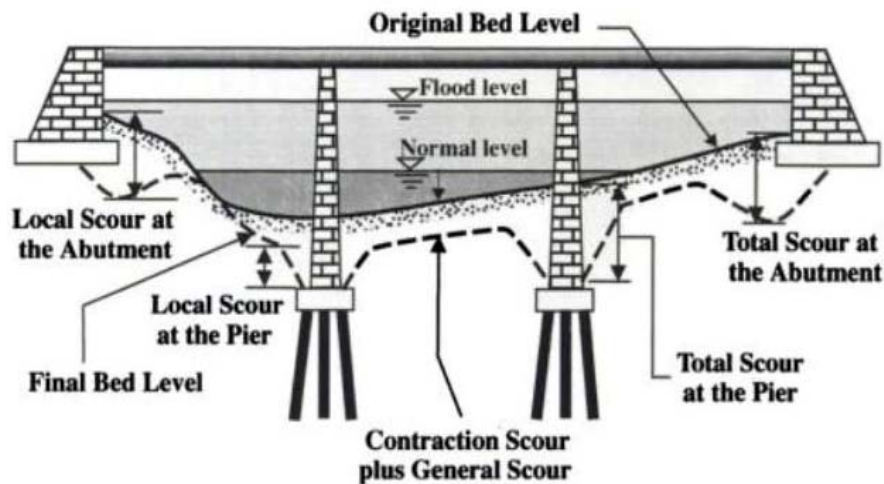


Figure 1.1 the types of scour that can occur at a bridge (Bruce W. M. and Stephen E. C., 2000).

1.3 Research Goal:

Many researchers had conducted a great number of experiments in laboratory flumes to investigate the local scour depth around a bridge pier (Ettema, 1980; Chiew and Melville, 1987; Lin, 1993). While multiple hazard situations involving scour and shaking can frequently occur, there had been no investigations into the effects of shaking motion on scouring around piers.

In the past, designs against multi-hazards of bridge structures, if considered, are often done by taking each hazard as separate and independent events. It may be reasonable to say that a large magnitude earthquake is not likely to occur at the same time as high wind forces with a 100-year recurrence cycle. While the correlation between earthquake and high wind is low, the correlation among other hazards could be higher. For instance, scouring is a continuous

phenomenon, and the traffic induced vibration is also continuous. It seems reasonable to considering these effects concurrently rather than as independent events. To investigate the possible synergistic effect of these combined hazards is the key goal of this research.

2. LITERATURE REVIEW

Numerical analyses on the prediction of soil displacement due to scour only and earthquake shaking only have been well documented, and the literatures review is shown below. The numerical method to predict the soil displacement due to scouring and shaking occurring concurrently, however, has not been developed.

2.1 The Flow Field around Piers Causing Local Scour

The flow field around a pier embedded in a loose sediment bed of an open channel is complex in nature, and the complexity increases with the development of flow separation around a scour hole to form a three-dimensional vortex at the base of the pier [4]. The flow field around piers has been well documented (Hjorth 1975; Melville 1975; Dey 1995; Dey *et al* 1995; Graf & Istiarto 2002). The principal features of the flow are the down-flow ahead of the pier. The down-flow is a consequence of flow deceleration ahead of the pier. The associated stagnation pressures on the face of the pier are highest near the surface, where the deceleration is greatest, and decreases from the surface down. The resulting downwards pressure gradient at the pier face generates the down-flow. The down-flow impinging on the bed acts like a vertical jet that erodes a groove immediately adjacent to the front of

the pier. The development of the scour hole around the pier creates a lee eddy, known as the horseshoe vortex. The down-flow and the horseshoe vortex together are primarily responsible for local scour. Wake vortices arise from flow separation at the sides of the pier. These vortices are translated downstream by the mean flow and act like vacuum machine sucking up sediment from the bed. The flow pattern and scour hole at a pier are illustrated in Figure 2.1.

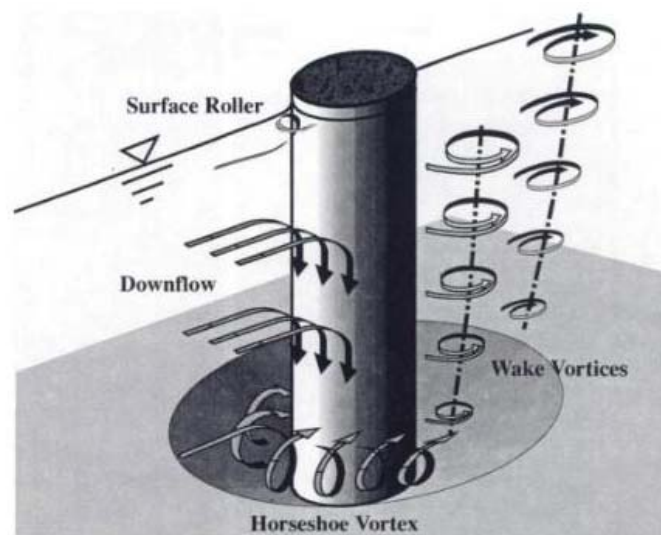


Figure 2.1 the flow and scour patterns at a circular pier. (Bruce W. M., Stephen E. C., 2000)

2.2 3-D Numerical Model of Scour around Circular Piers

Yen *et al.* (2000) developed a morphological model consisting of a 3-D scour model to simulate the bed evolution around a circular pier. For the scour model, the gravity effect of the sloping bed of the local scour hole is combined as part of the effective bed shear stress. To apply the sediment transport formula in the

scour hole with a sloping bed, the gravitational component along the bed surface is considered as a part of the effective shear stress impelling the motion of the sediment particles. The effective shear stress can be expressed by van Rijn's bed-load transport formula as:

$$\tau_{be} = \tau_b \times \cos(\beta - \delta) + w' \times \sin \theta \times \cos(\alpha_d - \delta) / A \quad (2.1)$$

Where τ_{be} is the effective shear stress; τ_b is the bed shear stress due to the flow motion; β is the angle between the direction of bed shear and the x-axis; δ is the angle between the direction of sediment motion and the x-axis, which can be evaluated using a method given elsewhere (Yen *et al.*, 1997); w' is the immersed weight of the sediment particle; θ is the angle of the local bed slope; α_d is the angle between the direction along the local sloping bed and the x-axis; and A is the projected area of the sediment particle[5].

Moreover, to simulate scour due to the down-flow in front of the pier, a relationship based on submerged jet flow scouring (Clarke, 1962) had been modified and employed. The experimental data of scour depths at the pier nose (R. Ettema, 1980) and bed elevation contours around a pier (G. H. Lin, 1993) were used to compare with simulated results (Yen *et al.*, 2000) to check the validity of the 3D model. The results showed good agreement between simulation and experimental results. In Figure 2.2, the simulated scour depth at

the pier nose as a function of time was compared with the measured data. Good agreement between simulation and experimental results was evident.

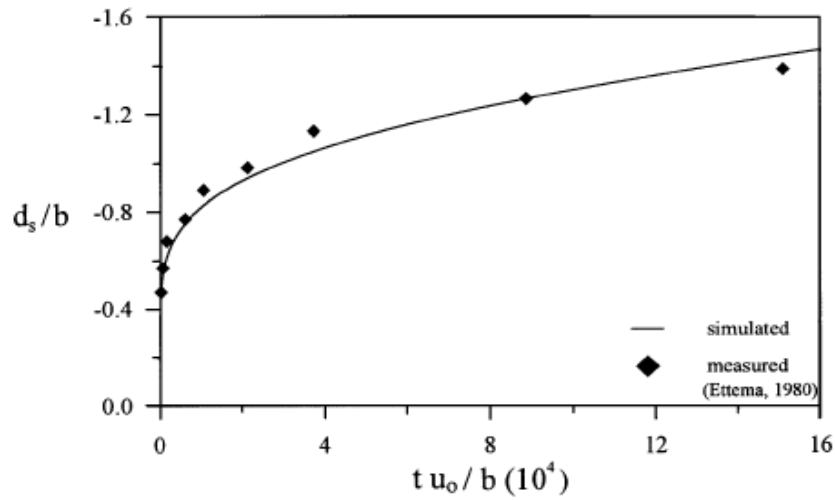


Figure 2.2 Comparison of simulated and experimental results of the scour depth evolution at the pier nose. (Yen et al., 2000)

Furthermore, the simulated and measured final bed elevation contours are shown in Figure 2.3 for comparison.

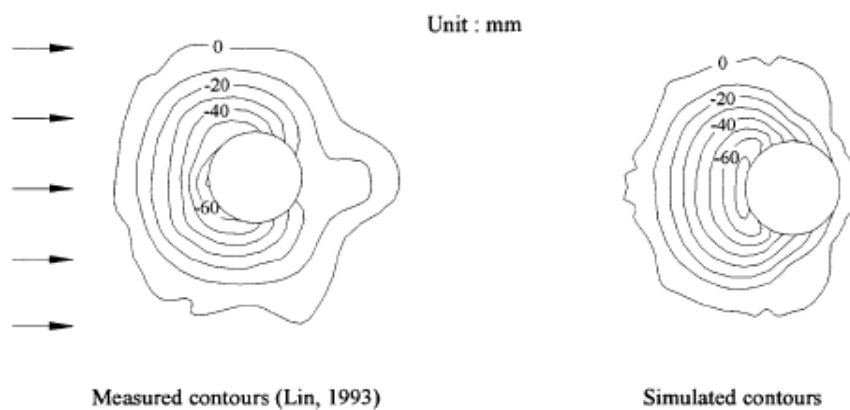


Figure 2.3 Comparison of measured and simulated final bed elevation contours. (Yen et al., 2000)

Although the simulated results of the scour pattern and maximum scour depths were satisfactory, the scour model developed by Yen *et al.* can only be used to predict the scour pattern. The present study is limited to the verification of the difference between conducting scour and shaking independently or concurrently. Therefore, Yen's 3-D scour model is not performed in the present study.

2.3 Methods for Predicting Slope Displacements Induced by Earthquake

In the present study, the simulated earthquake is applied after or along with scour. The simulated earthquake occurs over a scoured foundation. Therefore, earthquake-induced slope displacement resembles the current problem approximately.

The ability to predict earthquake-induced landslide displacements is important for many types of seismic-hazard analysis. Therefore, a brief review of some published methods to predict earthquake-induced slope displacements is shown below.

Newmark developed a procedure for estimating deformations in inclined ground during an earthquake. According to this method, the initial failure of slope occurs when the seismic forces are strong enough to exceed its sliding resistance. Newmark's method is based on a sliding block using a simple

equation of rectilinear motion under the action of a time-dependent force. The calculation is based on the assumption that the whole moving mass is displaced as a rigid body with mobilized resistance along a sliding surface.

Newmark's sliding block method can be represented by Figure 2.4.

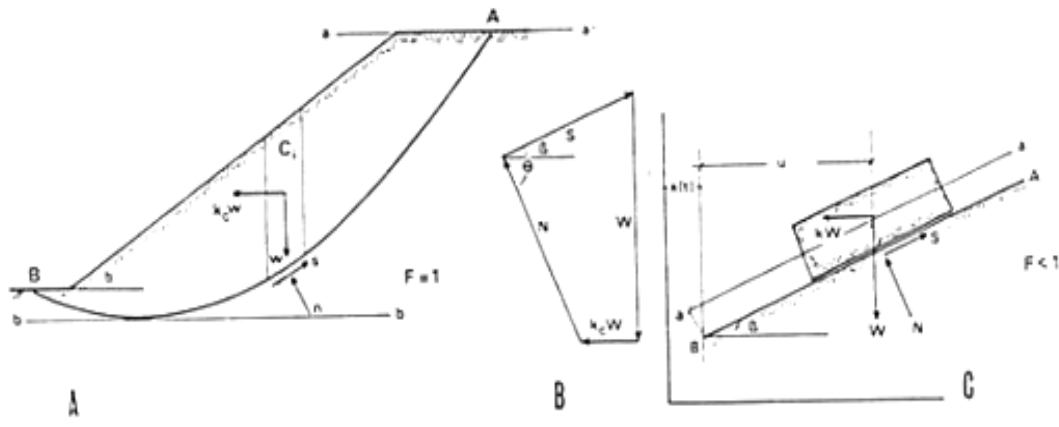


Figure 2.4 Application of simplified sliding block method for the stability analysis of slopes. For $k > k_c$, sliding takes place on plane AB inclined to the horizontal by an angle β . (Ambraseys & Menu, 1988)

In Figure 2.4, $k_c \cdot g$ indicates the minimum ground acceleration required to cause failure of a slope. The displacement can be determined by calculating the acceleration at which the mass starts moving, and the total displacement can be obtained by adding the displacements during the seismic period.

Liquefaction-induced lateral spreading is another direction of thinking to predict the earthquake-induced slope displacement. Soil Liquefaction is a phenomenon in which the strength and stiffness of soil is reduced by earthquake shaking or other rapid loading. A lateral spreading is defined as the mostly horizontal movement of gently sloping ground (less than 5% surface

slope). Liquefaction occurs in saturated soils. Prior to an earthquake, the water pressure between soil particles is relatively low. However, earthquake shaking can cause the water pressure between soil particles to increase to the point where the soil particles can readily move with respect to each other.

Hamada *et al.* (1987) developed a simple empirical model for horizontal displacements from studies of lateral spreading using data from Niigata and Noshiro, Japan, and the San Fernando Valley, California. By using site cross sections, mean values of relevant parameters were compiled for segments with similar displacement patterns, slopes, and soil conditions. Based on 60 cases, mostly from Noshiro, a regression equation was obtained (Hamada et al. 1987)

$$D = 0.75\sqrt{H}\sqrt[3]{\theta} \quad (2.2)$$

Where D is the horizontal displacement (m) and H is the thickness (m) of liquefied soil. When more than one soil layer liquefies, H is measured as the distance from the top-most to the bottom-most liquefied soil including all intermediate soil layers. θ is the slope (%) of either the ground surface or the base of the liquefied soil, whichever is greater.

Equation (2.2) is a fair fit to the data compiled by Hamada and his co-workers. However, this database is biased to the lateral spreading at Noshiro. The accuracy of the fitted equation outside these confines is unknown; therefore,

the usefulness of Hamada's empirical model is limited [7].

Other empirical models had been developed (Youd and Perkins, 1987; Bartlett and Youd, 1995). Their accuracy, however, was difficult to judge because the reliability of the fitted equations beside their confines was unknown.

Although the predictions of scour result and soil displacement due to earthquake were well documented, the prediction of the result due to these combined hazards has not yet been covered before. Since the combined effect of scouring and shaking is a complex nonlinear problem that is not addressed by analytical methods, the present study aims to experimentally verify the possibility of the synergistic effect between scouring and shaking.

3. SCOUR WITH HARMONIC SHAKING EXPERIMENT

3.1 Experimental Setup:

The experiments were conducted in the hydraulics laboratory of the Federal Highway Administration (FHWA) at McLean, Virginia. The FHWA designed and installed a flume at the Turner-Fairbank Highway Research Center (TFHRC). The flume where the experiments were carried out is 10cm wide, 2m long, 20cm deep, and weighted 240N. The size of the pier model was made out of a 4 inch x4 inch aluminum plate 1inch thick, a 5-½ inch long aluminum shaft with a ½ inch diameter. Two linear motors (BLMC-92-A manufactured by Aerotech) which have a peak payload capacity of 1540N were mounted into the flume to shake the entire streambed and pier as a unit, and the direction of oscillation is perpendicular to the flow of the water in the flume. A picture of the shaking motors is shown in the Figure 3.1. The shaking streambed is designed to have maximum displacement amplitude of 1.2 cm. During testing, the displacement amplitude is limited to 1.0 cm. The smaller limit is used to allow for some error in the controlled displacement. A picture of the shaking streambed and pier model is shown in the Figure 3.2.



Figure 3.1 the shaking flume.

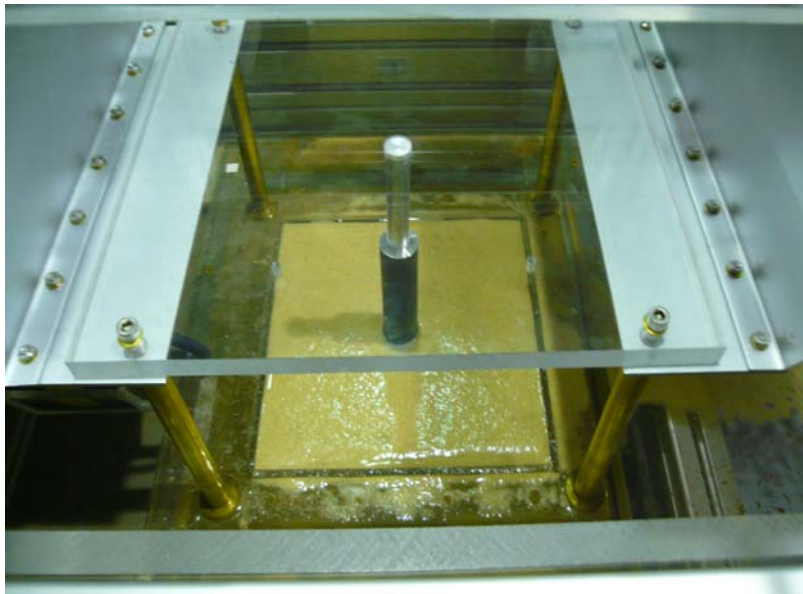


Figure 3.2 Shaking streambed and pier.

A simple method to obtain the amount of scouring is to use a distance measurement device to measure the distance to the sand surface. Distance measurement is made by using a laser distance sensor. The sensor projects a laser to the surface, and then calculates the time of travel to obtain the distance.

The sensor is capable of a measurement accuracy of 0.01mm. The sensor is placed on a robot arm that that can move in longitudinal and transverse directions of the flume to allow the sensor projects laser over the shaking streambed. The motor which controls the robot arm is placed as close to the shaking streambed as possible. The robot arm and the positioning motor are shown in the figures below.

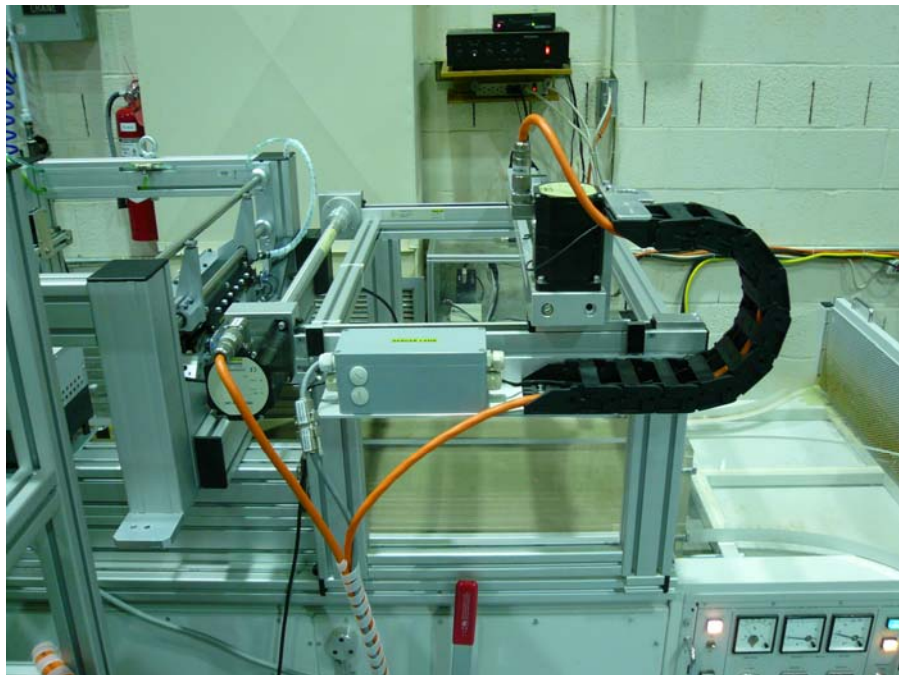


Figure 3.3 the robot arm and positioning motor for the harmonic shaking experiment.

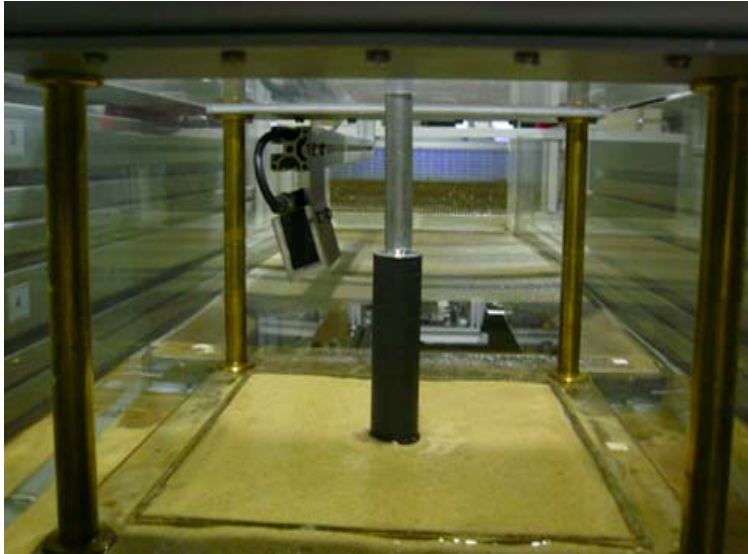


Figure 3.4 the laser displacement sensor for the harmonic shaking experiment.

The size of the laser displacement sensor is $1\text{cm} \times 3\text{cm} \times 5\text{cm}$. The laser is housed in an acrylic box which is 2 cm thick. Therefore, if the laser measures the distance normally to the plane, the closest distance of measure point to the center of the pier is 2 cm . In order to measure the points around the pier, we placed the laser at an angle of $\alpha = 18.5^\circ$. Given this angle, the position along the transverse direction is not the same if the depth of the sand is changed. This can be adjusted by moving in the transverse direction:

Away from the centerline by $(d_{\text{current}} - d_0)\sin \alpha$, if $d_{\text{current}} > d_0$

Toward the centerline by $(d_{\text{current}} - d_0)\sin \alpha$, if $d_{\text{current}} < d_0$

Where d_{current} is the current depth and d_0 is the depth at the beginning of the

experiment. d_{current} changes as the laser moves. Therefore, additional adjustment needs to be made in the transverse direction. The movement is convergent as long as the change of depth is not great. In other words, the movement converges as long as the surface of the sand is smooth. This condition is satisfied for all tests performed.

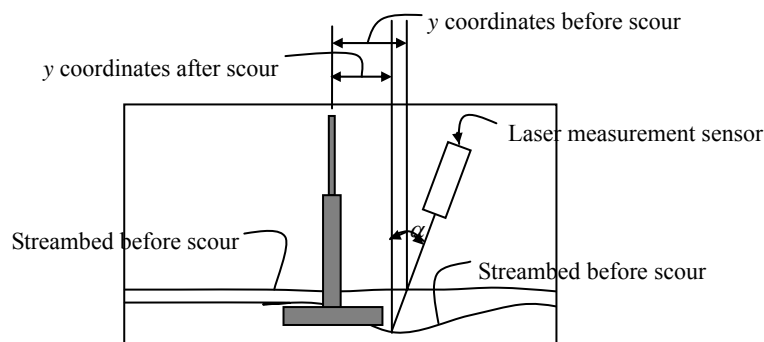


Figure 3.5 laser measurement sensor positioning.

The procedure to measure the scour surface is then reduced to measuring the scour depth at a set of predetermined points on the surface of the sand. The scour surface is assumed to be symmetric with respect to the centerline of the flume. Hence only one half of the surface is measured. This facilitates the measurement sensor positioning on the robot arm, as the sensor is positioned at an angle, and measurements on the other side of the flume cannot be made close to the centerline without changing the sensor position on the robot arm. The measurements are made by recording the depth immediately after the sand surface is manually flattened. Then the experiments for scouring and shaking

are performed as appropriate, and the depths at the same locations are measured and compared. Figure 3.5 shows a typical view of the sand surface after it is manually flattened, and after a scouring experiment.

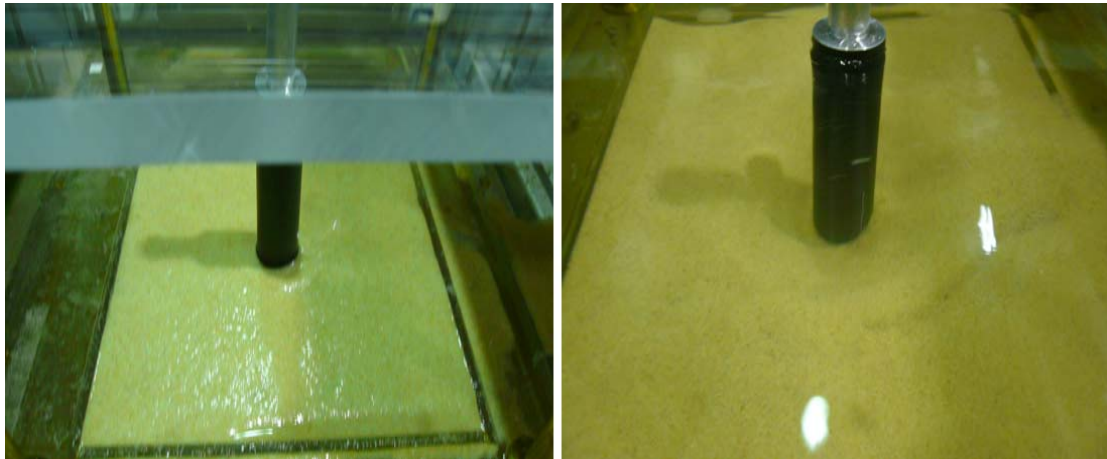


Figure 3.6 the surface of the streambed before and after a scouring experiment.

Using x to denote the longitudinal direction, and y to denote the transverse direction, the depths at the following points are measured:

Table 3.1 coordinates of points at which the depths are measured.

x (Longitudinal, mm)	y (Transverse, mm)
8.5	13
8.5	11
11.5	13
11.5	11
14.5	15
14.5	13
17.5	15
17.5	13
20.5	15
20.5	13
23.5	13
26.5	13
26.5	11

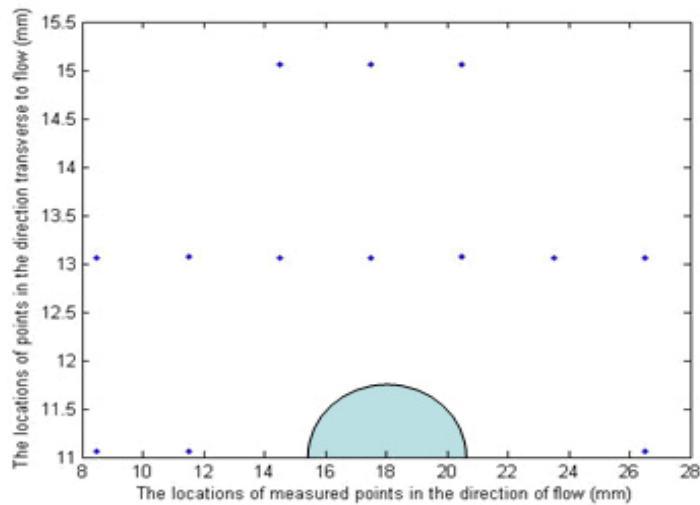


Figure 3.7 the location of points around the pier where the depths are measured.

3.2 Experiment procedure:

The main goal of the experiment is to verify the combined effects of scouring and harmonic shaking. In particular, we want to verify the possibility of synergistic effects. Therefore, we would like to compare the effects of scouring and harmonic shaking applied simultaneously and the sum of the effects of scouring and harmonic shaking applied sequentially. For the test applied flow and shaking concurrently (called concurrent test), we observed the results after applying scouring and shaking concurrently for a duration of 1 minute. For the test applied flow and shaking sequentially (called sequential test), we superimposed the effects of scouring and shaking by applying scouring and

shaking sequentially for the same duration of 1 minute each.

The following test procedures are followed:

1. The sand surface is manually smoothed with a straight edge. The surface depths at predetermined coordinates are measured.
2. Scouring is performed at a specified flow rate for 1 minute. The surface depths at predetermined coordinates are measured.
3. Shaking at specified amplitude and frequency for 1 minute. The surface depths at predetermined coordinates are measured.
4. Scouring at the specified flow rate again for 5 minutes. The surface depths at predetermined coordinates are measured.
5. The sand surface is manually smoothed with a straight edge again. The surface depths at the predetermined coordinates are measured.
6. Scouring and shaking at specified flow rate and shaking frequency and amplitude are performed simultaneously for 1 minute, and then the surface depths at the predetermined coordinates are measured.

An initial test was performed using a water depth of 8 *cm* in the flume, a flow speed of 18 *cm/s*, and shaking frequency of 2 *Hz* for 1 minute. The frequency was adjusted manually to the maximum value that the motor can accommodate.

In this experiment, the maximum amplitude of 1 *cm* was used. Visual

observations indicated that scouring did not appear to have been influenced by the shaking. The frequency of shaking was too low, and the scouring for this experiment was insufficient to show the effect of either phenomenon. Based on this preliminary test, the fluid flow was increase to the vicinity of the critical flow for settlement transport. And the shaking frequencies were increased to 9 Hz. The critical flow is calculated by using the empirical formula found in Hydraulic Engineering Circular No. 18 (Richardson and Davis, 2001):

$$Q_c = 11.25 D_m^{1/3} y_1^{1/6} \quad (3.1)$$

Where

Q_c = critical velocity in ft/s,

$D_m = 1.25 D_{50}$ in ft,

$D_{50} = 0.3\text{mm}$,

y_1 = depth of flow prior to scour in ft.

The frequencies and flow rate combinations tested in the present phase of the study is shown in the table below.

Table 3.2 the combination of shaking frequencies and flow rate used for experiments.

Flow (cm/s)	7 Hz	8 Hz	9 Hz
24	24cms7hz	24cms8hz	24cms9hz
25	25cms7hz	25cms8hz	25cms9hz
26	26cms7hz	26cms8hz	26cms9hz
27	27cms7hz	27cms8hz	27cms9hz
28	28cms7hz	28cms8hz	28cms9hz

3.3 Result Observations

The depth readings after each stage of the experiments described in the Test Protocols are listed in the tables below. The readings are in *cm*. Positive values denote a surface higher than the original surface of the streambed (a mound), and negative values represent surface lower than the original surface of the streambed (a hole).

Table 3.3 the depth readings of test 24cms7hz

Point	x projection (cm)	y projection (cm)	1 (cm)	2 (cm)	3 (cm)	4 (cm)	5 (cm)	6 (cm)
1	8.5	13	0.056	0.086	0.09	0.106	0.046	0.055
2	8.5	11	0.031	0.049	0.06	0.065	0.008	0.017
3	11.5	13	-0.016	0.011	0.102	0.12	0.029	0.059
4	11.5	11	-0.013	0.06	0.246	0.354	0.007	0.065
5	14.5	15	-0.027	0.297	0.384	0.627	0.02	0.195
6	14.5	13	-0.001	1.194	1.165	1.641	0.043	1.174
7	17.5	15	-0.036	0.663	0.717	1.179	0.051	0.732
8	17.5	13	-0.03	2.036	1.852	2.444	0.011	2.038
9	20.5	15	-0.096	0.041	0.105	0.433	0.013	0.282
10	20.5	13	-0.058	0.66	0.623	1.217	0.021	0.859
11	23.5	13	-0.05	-0.733	-0.66	-0.387	-0.031	-0.433
12	26.5	13	-0.095	-1.132	-1.026	-1.325	-0.093	-1.194
13	26.5	11	-0.06	-1.317	-1.318	-1.325	-0.105	-1.322

Table 3.4 the depth readings of test 24cms8hz

Points	x projection (cm)	y projection (cm)	1 (cm)	2 (cm)	3 (cm)	4 (cm)	5 (cm)	6 (cm)
1	8.5	13.062	0.042	0.055	0.056	0.054	0.024	0.065
2	8.5	11.062	0.039	0.048	0.062	0.063	0.028	0.052
3	11.5	13.064	0.03	0.049	0.187	0.178	0.012	0.165
4	11.5	11.066	-0.043	0.019	0.31	0.335	-0.009	0.234
5	14.5	15.063	-0.042	0.089	0.337	0.574	0.023	0.412
6	14.5	13.064	-0.026	1.229	1.079	1.609	0.003	1.24
7	17.5	15.063	0.002	0.619	0.57	1.067	0.031	0.811
8	17.5	13.062	-0.023	2.029	1.816	2.435	0.014	2.098
9	20.5	15.063	-0.039	0.046	0.094	0.226	-0.005	0.432
10	20.5	13.067	-0.017	0.631	0.508	1.162	0.021	0.988
11	23.5	13.066	-0.062	-0.747	-0.464	-0.534	-0.047	-0.117
12	26.5	13.065	-0.078	-1.078	-0.795	-1.314	-0.11	-0.972
13	26.5	11.068	-0.099	-1.319	-1.019	-1.32	-0.106	-1.071

Table 3.5 the depth readings of test 24cms9hz

Points	x projection (cm)	y projection (cm)	1 (cm)	2 (cm)	3 (cm)	4 (cm)	5 (cm)	6 (cm)
1	8.5	13	0.027	0.03	0.195	0.19	0.014	0.399
2	8.5	11	0.004	-0.003	0.173	0.179	0.009	0.4
3	11.5	13	-0.013	0.01	0.409	0.398	0.013	0.781
4	11.5	11	0.008	0.034	0.49	0.491	0.018	0.821
5	14.5	15	-0.015	0.057	0.357	0.362	-0.007	0.755
6	14.5	13	-0.044	1.19	0.643	1.324	0.005	1.15
7	17.5	15	0.025	0.591	0.385	0.629	0.031	0.63
8	17.5	13	-0.095	2.104	0.84	2.15	-0.01	1.293
9	20.5	15	0.007	-0.011	0.123	0.034	0.017	0.148
10	20.5	13	-0.031	0.692	0.17	0.762	0.002	0.176
11	23.5	13	-0.062	-0.764	-0.065	-0.66	-0.051	-0.022
12	26.5	13	-0.094	-0.994	-0.254	-0.766	-0.092	-0.498
13	26.5	11	-0.09	-1.311	-0.275	-1.319	-0.077	-0.465

Table 3.6 the depth readings of test 25cms7hz

Points	x projection (cm)	y projection (cm)	1 (cm)	2 (cm)	3 (cm)	4 (cm)	5 (cm)	6 (cm)
1	8.5	13	0.014	0.049	0.05	0.059	0.014	0.022
2	8.5	11	0.049	0.078	0.087	0.082	0.028	0.046
3	11.5	13	0.017	0.06	0.117	0.178	0.02	0.078
4	11.5	11	-0.011	0.127	0.229	0.449	-0.024	0.129
5	14.5	15	-0.033	0.238	0.348	0.629	-0.001	0.408
6	14.5	13	-0.029	1.269	1.176	1.756	0.039	1.381
7	17.5	15	-0.031	0.831	0.763	1.236	0.017	0.918
8	17.5	13	-0.013	2.112	2.026	2.481	0.026	2.221
9	20.5	15	-0.067	0.069	0.099	0.397	-0.022	0.372
10	20.5	13	-0.042	0.732	0.646	1.243	-0.021	1.035
11	23.5	13	-0.1	-0.776	-0.705	-0.399	-0.084	-0.294
12	26.5	13	-0.108	-1.325	-1.284	-1.326	-0.131	-1.189
13	26.5	11	-0.111	-1.325	-1.328	-1.328	-0.099	-1.326

Table 3.7 the depth readings of test 25cms8hz

Points	x projection (cm)	y projection (cm)	1 (cm)	2 (cm)	3 (cm)	4 (cm)	5 (cm)	6 (cm)
1	8.5	13	0.019	0.017	0.033	0.036	0.043	0.128
2	8.5	11	0.028	0.029	0.037	0.04	0.048	0.108
3	11.5	13	0.012	0.02	0.164	0.151	0.026	0.275
4	11.5	11	0.008	0.024	0.33	0.317	0.012	0.363
5	14.5	15	-0.024	0.283	0.426	0.677	0.019	0.451
6	14.5	13	0.003	1.3	1.181	1.675	0.032	1.372
7	17.5	15	0	0.817	0.68	1.253	0.01	0.897
8	17.5	13	0.005	2.077	1.958	2.508	0.041	2.188
9	20.5	15	-0.023	0.058	0.127	0.361	-0.023	0.513
10	20.5	13	0.001	0.749	0.516	1.26	0.021	1.166
11	23.5	13	-0.062	-0.734	-0.439	-0.427	-0.021	0.012
12	26.5	13	-0.069	-1.291	-0.876	-1.322	-0.08	-0.843
13	26.5	11	-0.097	-1.31	-1.043	-1.326	0.046	-0.977

Table 3.8 the depth readings of test 25cms9hz

Points	x projection (cm)	y projection (cm)	1 (cm)	2 (cm)	3 (cm)	4 (cm)	5 (cm)	6 (cm)
1	8.5	13	0.03	0.079	0.349	0.322	0.054	0.411
2	8.5	11	0.019	0.07	0.382	0.354	0.038	0.404
3	11.5	13	-0.001	0.032	0.513	0.507	0.006	0.854
4	11.5	11	-0.005	0.052	0.631	0.614	0.015	0.886
5	14.5	15	0.011	0.25	0.41	0.423	0.03	0.857
6	14.5	13	0.018	1.367	0.713	1.474	0.008	1.315
7	17.5	15	0.039	0.996	0.374	0.96	0.034	0.795
8	17.5	13	0.019	2.206	0.724	2.234	0.013	1.449
9	20.5	15	-0.012	0.183	0.109	0.094	-0.003	0.317
10	20.5	13	0.004	0.864	0.121	0.95	-0.022	0.312
11	23.5	13	-0.065	-0.578	0.009	-0.576	-0.018	0.104
12	26.5	13	-0.114	-1.311	-0.141	-0.783	-0.074	-0.345
13	26.5	11	-0.123	-1.315	-0.122	-1.319	-0.085	-0.362

Table 3.9 the depth readings of test 26cms7hz

Points	x projection (cm)	y projection (cm)	1 (cm)	2 (cm)	3 (cm)	4 (cm)	5 (cm)	6 (cm)
1	8.5	13	0.141	0.054	0.062	0.055	0.091	0.054
2	8.5	11	0.117	0.072	0.086	0.081	0.025	0.047
3	11.5	13	0.066	0.172	0.177	0.18	0.07	0.226
4	11.5	11	0.052	0.174	0.252	0.388	0.082	0.454
5	14.5	15	0.068	0.635	0.653	0.962	0.019	0.505
6	14.5	13	0.056	1.554	1.543	1.963	0.052	1.579
7	17.5	15	-0.025	1.187	1.205	1.54	-0.151	1.066
8	17.5	13	-0.023	2.394	2.358	2.868	-0.06	2.372
9	20.5	15	0.066	0.378	0.402	0.797	0.019	0.512
10	20.5	13	0.035	1.224	1.213	1.644	-0.038	1.249
11	23.5	13	0.462	-0.335	-0.318	-0.015	0.013	-0.158
12	26.5	13	0.201	-0.89	-0.845	-1.043	-0.023	-1.022
13	26.5	11	0.355	-1.322	-1.319	-1.32	-0.009	-1.168

Table 3.10 the depth readings of test 26cms8hz

Points	x projection (cm)	y projection (cm)	1 (cm)	2 (cm)	3 (cm)	4 (cm)	5 (cm)	6 (cm)
1	8.5	13	0.033	0.034	0.034	0.029	0.096	0.076
2	8.5	11	0.008	0.002	0.002	0.005	0.038	0.074
3	11.5	13	0.044	0.036	0.286	0.277	0.107	0.323
4	11.5	11	-0.201	0.044	0.489	0.495	0.06	0.59
5	14.5	15	0.164	0.509	0.583	0.98	0.031	0.626
6	14.5	13	0.032	1.538	1.447	1.933	0.063	1.632
7	17.5	15	0.164	1.128	1.059	1.5	0.011	1.159
8	17.5	13	0.154	2.537	2.305	2.76	-0.004	2.388
9	20.5	15	0.226	0.421	0.462	0.74	0.035	0.711
10	20.5	13	0.17	1.185	0.981	1.515	0.043	1.4
11	23.5	13	0.009	-0.314	-0.152	-0.05	0.015	0.149
12	26.5	13	-0.019	-0.824	-0.669	-0.98	-0.033	-0.77
13	26.5	11	-0.084	-1.318	-1.01	-1.32	-0.043	-0.907

Table 3.11 the depth readings of test 26cms9hz

Points	x projection (cm)	y projection (cm)	1 (cm)	2 (cm)	3 (cm)	4 (cm)	5 (cm)	6 (cm)
1	8.5	13	0.035	0.026	0.128	0.126	0.081	0.324
2	8.5	11	0.04	0.04	0.143	0.132	0.078	0.32
3	11.5	13	0.068	0.097	0.497	0.51	0.086	0.918
4	11.5	11	0.019	0.165	0.684	0.682	0.096	1.056
5	14.5	15	0.033	0.603	0.523	1.022	0.085	1.058
6	14.5	13	0.021	1.542	1.052	2.134	0.103	1.664
7	17.5	15	0.005	1.149	0.582	1.612	0.051	1.109
8	17.5	13	-0.001	2.307	1.444	2.991	0.093	2.178
9	20.5	15	0.038	0.324	0.307	0.821	0.043	0.743
10	20.5	13	0.03	1.095	0.505	1.687	0.058	1.238
11	23.5	13	0.016	-0.43	0.045	-0.016	0.016	0.397
12	26.5	13	-0.037	-1.069	-0.276	-1.027	-0.051	-0.272
13	26.5	11	-0.028	-1.308	-0.291	-1.24	-0.043	-0.347

Table 3.12 the depth readings of test 27cms7hz

Points	x projection (cm)	y projection (cm)	1 (cm)	2 (cm)	3 (cm)	4 (cm)	5 (cm)	6 (cm)
1	8.5	13	0.274	0.263	0.264	0.266	0.241	0.198
2	8.5	11	0.192	0.185	0.19	0.173	0.041	0.062
3	11.5	13	0.242	0.459	0.474	0.581	0.229	0.488
4	11.5	11	0.252	0.46	0.525	0.757	0.077	0.651
5	14.5	15	0.097	0.86	0.864	1.22	0.085	0.836
6	14.5	13	0.102	1.71	1.668	2.093	0.185	1.732
7	17.5	15	0.018	1.267	1.227	1.682	0.024	1.33
8	17.5	13	0.021	2.349	2.331	2.94	0.138	2.399
9	20.5	15	0.016	0.464	0.525	0.938	0.386	0.743
10	20.5	13	-0.01	1.309	1.277	1.847	0.367	1.435
11	23.5	13	0.012	-0.29	-0.262	0.191	0.094	0.052
12	26.5	13	-0.104	-1.005	-0.989	-0.907	-0.071	-0.751
13	26.5	11	-0.097	-1.307	-1.305	-1.3	-0.06	-1.049

Table 3.13 the depth readings of test 27cms8hz

Points	x projection (cm)	y projection (cm)	1 (cm)	2 (cm)	3 (cm)	4 (cm)	5 (cm)	6 (cm)
1	8.5	13	0.129	0.027	0.041	0.054	0.035	0.127
2	8.5	11	0.131	0.041	0.046	0.069	0.063	0.131
3	11.5	13	0.064	0.191	0.412	0.491	0.089	0.452
4	11.5	11	0.124	0.412	0.66	0.805	0.05	0.686
5	14.5	15	0.043	0.853	0.788	1.317	0.076	0.786
6	14.5	13	0.043	1.704	1.565	2.379	0.078	1.746
7	17.5	15	0.019	1.28	1.232	1.905	-0.004	1.217
8	17.5	13	0.078	2.42	2.379	3.232	-0.018	2.564
9	20.5	15	0.058	0.59	0.588	1.178	0.008	0.831
10	20.5	13	0.075	1.332	1.197	1.945	0.004	1.538
11	23.5	13	0.054	-0.19	-0.075	0.41	-0.047	0.281
12	26.5	13	-0.024	-1.032	-0.934	-0.751	-0.091	-0.69
13	26.5	11	-0.011	-1.309	-1.08	-1.183	-0.092	-0.679

Table 3.14 the depth readings of test 27cms9hz

Points	x projection (cm)	y projection (cm)	1 (cm)	2 (cm)	3 (cm)	4 (cm)	5 (cm)	6 (cm)
1	8.5	13	0.04	0.061	0.275	0.272	0.033	0.462
2	8.5	11	0.065	0.088	0.32	0.294	0.062	0.465
3	11.5	13	0.017	0.092	0.631	0.622	0.107	1.033
4	11.5	11	0.086	0.318	0.772	0.767	0.123	1.139
5	14.5	15	0.051	0.621	0.533	0.722	0.077	1.153
6	14.5	13	0.048	1.544	1.001	1.828	0.116	1.678
7	17.5	15	-0.02	1.059	0.496	1.251	0.022	1.117
8	17.5	13	-0.046	2.324	0.941	2.516	0.077	2.099
9	20.5	15	-0.027	0.408	0.245	0.403	0.042	0.766
10	20.5	13	-0.037	1.143	0.298	1.365	0.064	0.944
11	23.5	13	-0.009	-0.408	0.078	-0.327	0.025	0.398
12	26.5	13	-0.051	-1.318	-0.161	-0.933	-0.052	-0.054
13	26.5	11	-0.026	-1.324	-0.153	-1.313	-0.056	-0.121

Table 3.15 the depth readings of test 28cms7hz

Points	x projection (cm)	y projection (cm)	1 (cm)	2 (cm)	3 (cm)	4 (cm)	5 (cm)	6 (cm)
1	8.5	13	0.048	0.043	0.054	0.066	0.109	0.086
2	8.5	11	0.027	-0.003	0.005	0.02	0.102	0.079
3	11.5	13	0.076	0.104	0.284	0.441	0.026	0.277
4	11.5	11	-0.017	0.319	0.515	0.788	0.065	0.49
5	14.5	15	0.058	0.736	0.827	1.24	0.04	0.766
6	14.5	13	0.108	1.721	1.638	2.2	0.019	1.747
7	17.5	15	0.034	1.337	1.269	1.787	0.064	1.284
8	17.5	13	0.054	2.688	2.459	3.079	-0.021	2.67
9	20.5	15	0.045	0.592	0.631	1.03	0.016	0.724
10	20.5	13	0.067	1.366	1.331	1.811	0.004	1.536
11	23.5	13	0.026	-0.208	-0.23	0.259	-0.054	0.089
12	26.5	13	-0.069	-1.119	-1.036	-0.807	-0.073	-0.958
13	26.5	11	-0.086	-1.319	-1.324	-1.226	0.007	-1.189

Table 3.16 the depth readings of test 28cms8hz

Points	x projection (cm)	y projection (cm)	1 (cm)	2 (cm)	3 (cm)	4 (cm)	5 (cm)	6 (cm)
1	8.5	13	0.103	0.041	0.06	0.087	0.043	0.15
2	8.5	11	0.056	0.045	0.049	0.078	0.034	0.136
3	11.5	13	0.1	0.159	0.476	0.493	0.04	0.516
4	11.5	11	0.077	0.264	0.652	0.741	0.06	0.668
5	14.5	15	0.053	0.626	0.754	1.211	0.038	0.779
6	14.5	13	0.068	1.734	1.497	2.113	0.034	1.675
7	17.5	15	-0.003	1.195	1.097	1.651	0.052	1.212
8	17.5	13	0.012	2.588	2.327	3.056	0.042	2.523
9	20.5	15	0.026	0.527	0.557	0.894	0.015	0.807
10	20.5	13	0.02	1.323	1.135	1.746	0.009	1.531
11	23.5	13	-0.024	-0.149	-0.051	0.158	-0.034	0.331
12	26.5	13	-0.086	-0.964	-0.727	-0.855	-0.123	-0.568
13	26.5	11	-0.044	-1.327	-0.958	-1.224	-0.093	-0.751

Table 3.17 the depth readings of test 28cms9hz

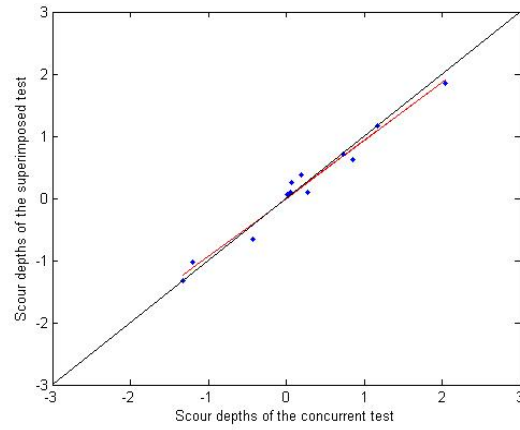
Points	x projection (cm)	y projection (cm)	1 (cm)	2 (cm)	3 (cm)	4 (cm)	5 (cm)	6 (cm)
1	8.5	13	0.027	0.066	0.191	0.186	0.084	0.591
2	8.5	11	0.059	0.074	0.202	0.195	0.041	0.589
3	11.5	13	0.023	0.04	0.588	0.579	0.04	1.189
4	11.5	11	0.017	0.255	0.775	0.772	0.012	1.285
5	14.5	15	-0.019	0.581	0.558	0.87	0.01	1.322
6	14.5	13	0.035	1.666	1.018	2.081	0	1.872
7	17.5	15	-0.011	1.223	0.591	1.47	0	1.32
8	17.5	13	0.011	2.627	1.322	2.719	-0.003	2.387
9	20.5	15	0.017	0.495	0.31	0.542	-0.037	0.985
10	20.5	13	0.018	1.234	0.466	1.564	-0.038	1.226
11	23.5	13	0.002	-0.264	0.102	-0.103	-0.095	0.564
12	26.5	13	-0.119	-1.193	-0.223	-1.004	-0.099	-0.004
13	26.5	11	-0.124	-1.323	-0.235	-1.307	-0.095	-0.096

3.4 Result Discussion

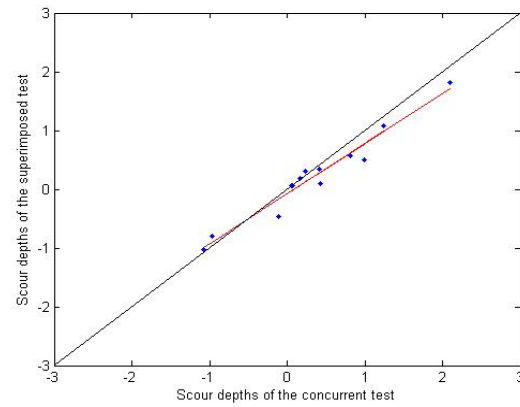
The purpose of the experiments is to verify if the effects of shaking and scouring can be superimposed. Our interests are their effects on the structure and the foundation. The present study is limited to study the effects of scouring and shaking on the foundation.

We want to compare the foundation surface if the effects of scour and shaking are the superposition of the individual tests with the surface if the same level of shaking and scour occur concurrently. To compare the results of the concurrent tests and the sequential tests, the data are plotted with the concurrent test results on the horizontal axis and the sequential test results on the vertical axis. If the results of the two sets of tests are identical, the points should lie on a straight line with a slope of 1. Deviation from this line represents difference of depths using the sequential tests and concurrent tests. Linear least square is used to fit the scattered data to obtain a relationship between the sequential test results and the concurrent test results. We place the results from the sixth test on the horizontal axis, because it is assumed to represent the actual event of shaking and scouring concurrently. The results of the third test are placed on the vertical axis. They represent an assumed procedure of shaking after the surface has been scoured. We will call this the sequential test procedure.

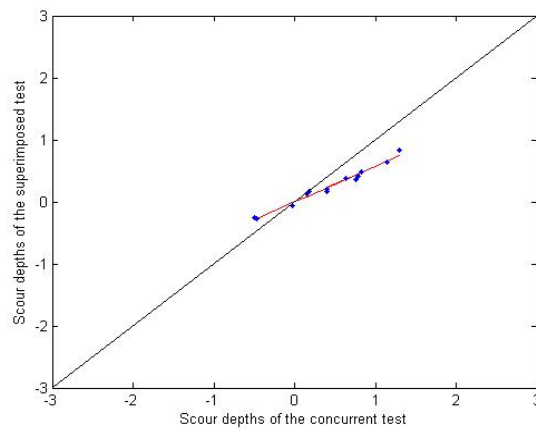
Points lying above this line mean that at those points, the sequential test results are greater than the depths obtained from the concurrent test. In other words, if the point is on a mound of soil deposit, then the depths from the sequential test are greater than the depths from the concurrent test. If the point is in a scoured hole, then the hole from the sequential test is shallower than the hole from the concurrent test at that point. Conversely, points lying below the line of unit slope have depths obtained from the sequential test smaller than the depths from the concurrent test. Shaking of a scoured surface would cause the deposit mounds to flatten, and the holes to fill. This result would be represented by a line with slope less than 1. A line entirely above the line with unit slope means that the mounds are higher, and holes are shallower. A line entirely below the line with unit slope means that the mounds are lower, and the holes are deeper. These depth comparisons are shown in Figures 3.8 to 3.12 for the tests performed at different flow rates and different shaking frequencies.



(a)

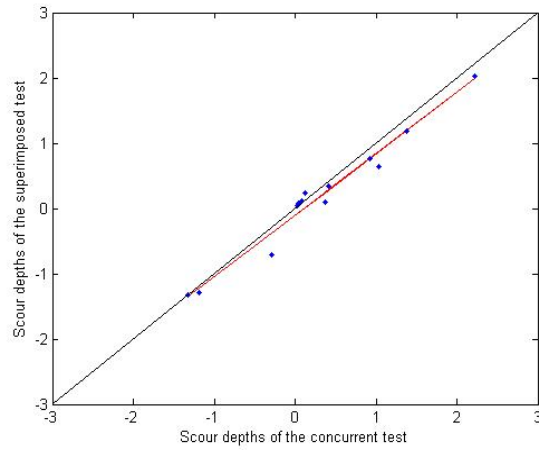


(b)

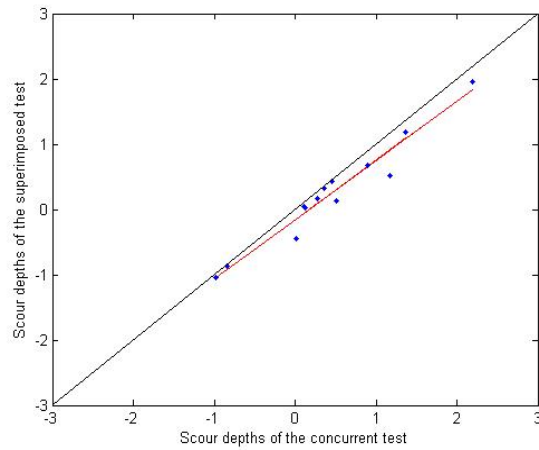


(c)

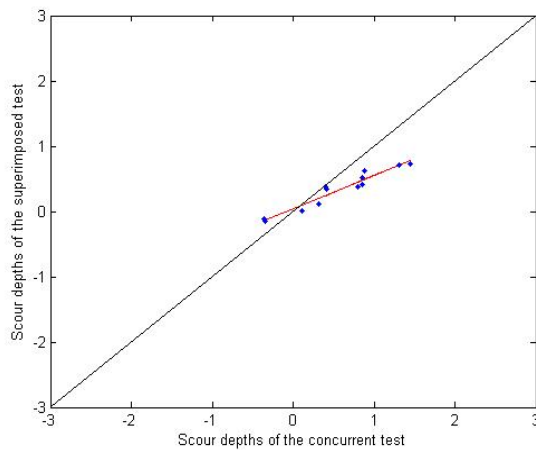
Figure 3.8 Scatter plots of the scour depths of the sequential (3rd) test versus concurrent (6th) test at a flow rate of 24cm/s and different harmonic shaking frequencies of: (a) 7Hz (b) 8Hz (c) 9Hz.



(a)

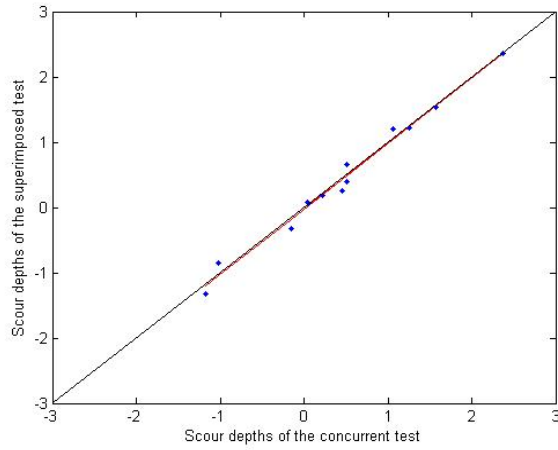


(b)

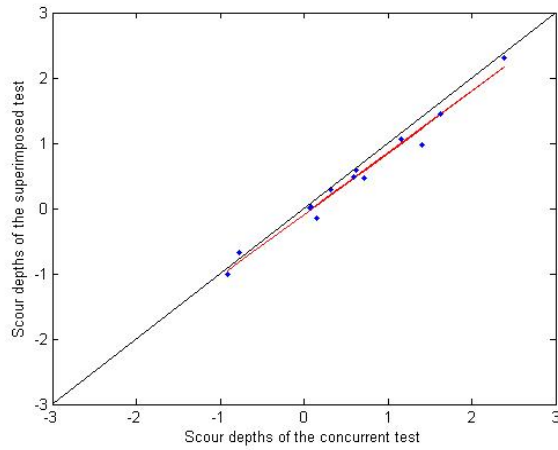


(c)

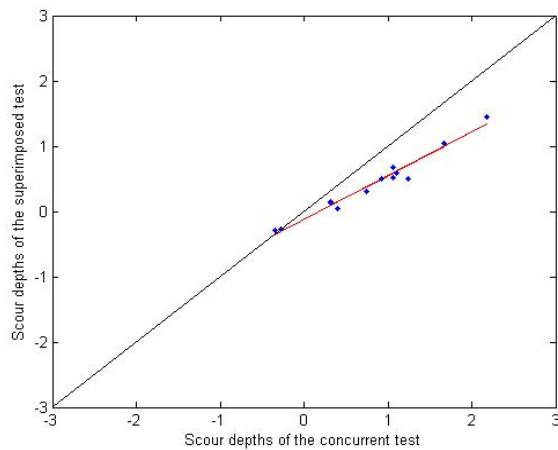
Figure 3.9 Scatter plots of the scour depths of the sequential (3rd) test versus concurrent (6th) test at a flow rate of 25cm/s and different harmonic shaking frequencies of: (a) 7Hz (b) 8Hz (c) 9Hz.



(a)

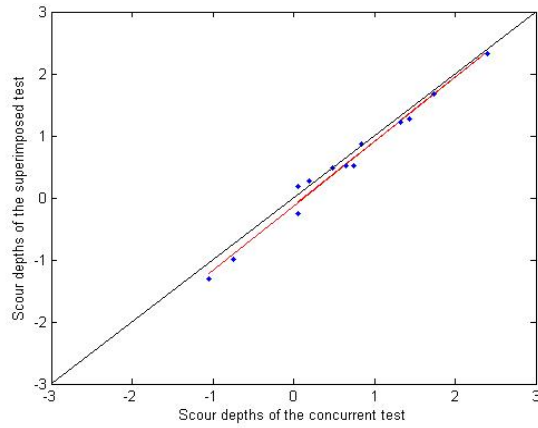


(b)

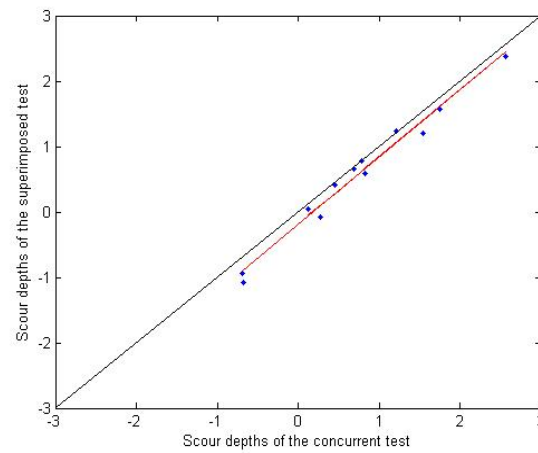


(c)

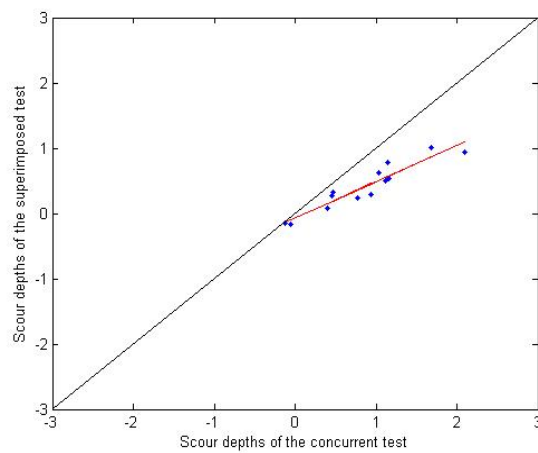
Figure 3.10 scatter plots of the scour depths of the sequential test (3rd) versus concurrent test (6th) with flow rate of 26cm/s and different harmonic shaking frequencies of: (a) 7Hz (b) 8Hz (c) 9Hz.



(a)

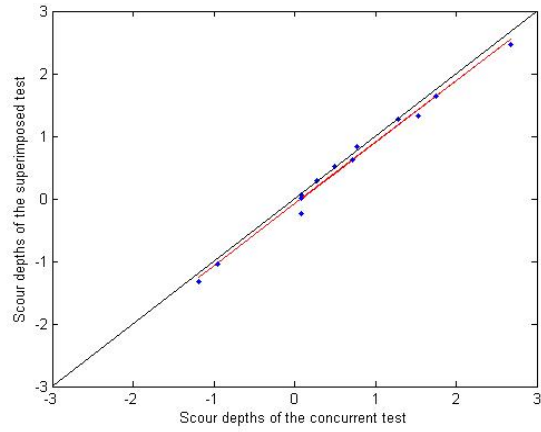


(b)

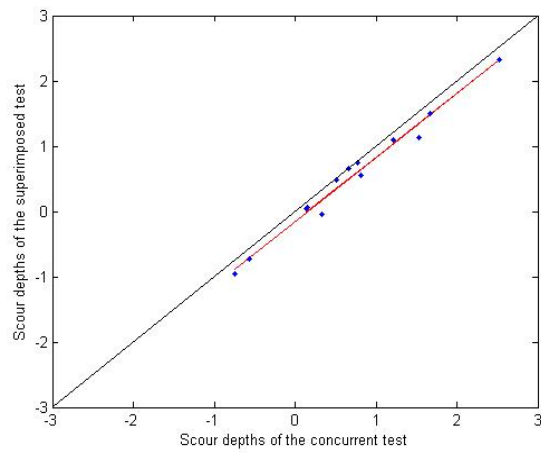


(c)

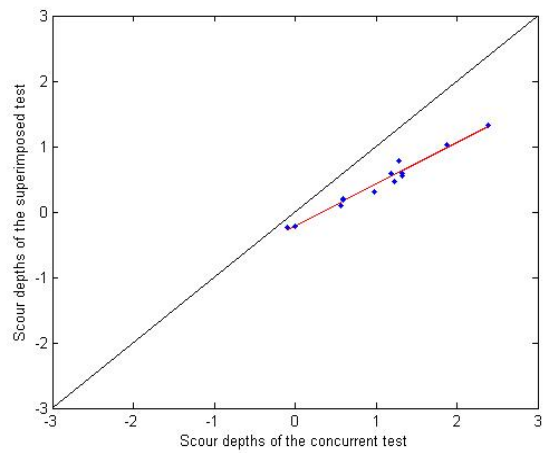
Figure 3.11 scatter plots of the scour depths of the sequential test (3rd) versus concurrent test (6th) with flow rate of 27cm/s and different harmonic shaking frequencies of : (a) 7Hz (b) 8Hz (c) 9Hz.



(a)



(b)



(c)

Figure 3.12 scatter plots of the scour depths of the sequential test (3rd) versus concurrent test (6th) with flow rate of 28cm/s and different harmonic shaking frequencies of: (a) 7Hz (b) 8Hz (c) 9Hz.

Figure 3.8 and 3.9 show that in general the sequential tests generate mounds that are lower, and holes that are shallower, and the difference of scour depths between concurrent test and sequential test increase as the shaking frequency increase. From the figure 3.10 to 3.12, we can see that at all three flow rates tested the difference between the concurrent tests and the sequential tests are considerably greater at the shaking frequency of 9 Hz. As for the 7 Hz and 8 Hz test, the fitted lines from test results are entire below and almost parallel to the line with unit slope, which means that the entire scoured surface of sequential test are lower than the scoured surface of concurrent test by the same amount.

To show the difference of scour depths between concurrent test and sequential test in a quantitative way, we use the root means square of the difference in measured data as a metric of the accuracy of the sequential test results.

Let $y_i = z_{3i} - z_{6i}$, in which z_{3i} represents the measured depth of the sequential tests, and z_{6i} represents the measured depth of the concurrent scour and shaking experiment. Then we can represent the magnitude of difference of the two approaches by the following equation:

$$x = \frac{1}{n} \sqrt{\sum_{i=1}^n y_i^2} \quad (3.1)$$

The root mean square of the differences among sequential tests and concurrent tests are listed in the table below.

Table 3.18 the root mean square of the scour depths differences among sequential tests and concurrent tests performed at different flow rates and different shaking frequencies.

Flow Rate	7Hz	8Hz	9Hz
24 cm/s	0.040	0.063	0.081
25 cm/s	0.060	0.075	0.098
26 cm/s	0.033	0.050	0.127
27 cm/s	0.046	0.060	0.148
28 cm/s	0.038	0.056	0.176

From the table 3.18 shown above, we found that the difference between the scour depths of the combined sequential tests and the concurrent tests are highly frequency dependent. The difference increases as the shaking frequency increases. Flow rate, however, does not appear to be a significant factor in the scour depth measurements obtained from the present experiment.

Another metric for comparison of the sequential and concurrent test results is the maximum scoured depth, because it is one of the most important measures for the foundation's safety level. To do the dimensional analysis, we divide the maximum scour depth (d in cm) by the pier diameter ($b = 1.27\text{ cm}$) to get the dimensionless results. Table 3.19 shows the comparison of the dimensionless maximum scoured depth between the two tests methods.

Table 3.19 the maximum scour depths (d/b) of the sequential tests and the concurrent tests.

Flow Rates (cm/s)	7Hz		8Hz		9Hz	
	sequential	concurrent	sequential	concurrent	sequential	concurrent
24	-1.038	-1.041	-0.802	-0.843	-0.217	-0.392
25	-1.046	-1.044	-0.821	-0.769	-0.111	-0.285
26	-1.039	-0.920	-1.010	-0.714	-0.229	-0.273
27	-1.028	-0.826	-0.795	-0.543	-0.127	-0.095
28	-1.043	-0.936	-0.754	-0.591	-0.185	-0.076

In table 3.19, we can easily observe that the maximum scour depths decrease as the frequencies increase in both sequential and concurrent conditions. This result is reasonable as shaking motion is expected to cancel the effects of scouring.

To quantify the influence of the shaking frequency, the percent difference of the sequential tests compared to the results of the concurrent test is calculated by:

$$\%Difference = \frac{|x_1 - x_2|}{|x_1|} \times 100\% \quad (3.2)$$

in which x_1 represents the actual value, and x_2 represents the compared value.

The concurrent test is assumed to represent the real event, therefore, x_1 is set as the maximum scour depths of the concurrent tests (6th tests) and x_2 as the maximum scour depths of sequential tests (3rd tests). The calculation results of percent difference are shown in Table 3.20.

Table 3.20 the percent difference of maximum scour depths of sequential tests vs. concurrent tests (%)

Flow Rates(cm/s)	7Hz	8Hz	9Hz
24	0.303%	4.855%	44.78%
25	0.151%	6.755%	61.05%
26	12.93%	11.36%	16.14%
27	24.40%	56.52%	33.06%
28	11.35%	27.56%	144.8%

From Table 3.20, the differences of the maximum scour depths for concurrent tests and sequential tests are highly frequency dependent. Interestingly, the percent differences do not appear to be dependent on the flow rates.

Point-wise comparison of scour depth, however, may not be a good indication of the overall difference in the surface contour, as the differences of depth are not the same at different locations. One way to account for the global difference is to compare the change in volume under the surface. The volume under the surface can be approximated at the points where the measurements are made, hence

$$V = \sum_{i=1}^n (Z_i \times dA_i) \quad (3.3)$$

where Z_i is the scour depths at the measured point, n is the number of measured points which is 120, and dA_i is the effective area of the measured point. The calculated scouring volumes of the sequential and the concurrent tests are

shown in Table 3.21.

Table 3.21 the scouring volumes (cm^3) of the sequential tests and the concurrent tests.

Flow Rates (cm/s)	7Hz		8Hz		9Hz	
	sequential	concurrent	sequential	concurrent	sequential	concurrent
24	18.024	17.694	13.668	12.960	3.564	5.91
25	19.902	16.854	14.148	10.920	1.578	4.242
26	14.892	14.088	10.986	10.062	3.402	3.714
27	15.336	10.800	12.534	8.214	1.884	1.050
28	14.160	12.882	10.416	7.914	2.748	0.600

Table 3.22 the percent difference of the scouring volumes of sequential tests vs. concurrent tests (%).

Flow Rates (cm/s)	7Hz	8Hz	9Hz
24	1.865%	5.463%	39.70%
25	18.08%	29.56%	62.80%
26	5.707%	8.183%	9.401%
27	42.00%	52.59%	79.43%
28	9.921%	31.61%	358.0%

Table 3.22 shows that the difference in volume also increases as the shake frequency increase from 7 to 9 Hz. The influence of flow rate is not as evident at the lower shaking frequencies. At 9 Hz, however, the flow rate shows a marked influence on the change in volume.

The maximum depth and total volume are good measures of the differences between the results, but they do not show the amount of scatter in the data. An

easy way to show the scatter is by using the correlation coefficient. The correlation coefficient $\rho_{x,y}$ between two random variables X and Y with expected values μ_x and μ_y and standard deviations σ_x and σ_y is defined as:

$$\rho_{x,y} = \frac{\text{cov}(X,Y)}{\sigma_x \sigma_y} = \frac{E[(X - \mu_x)(Y - \mu_y)]}{\sigma_x \sigma_y} \quad (3.4)$$

Where E is the expected value operator and cov(X, Y) means covariance.

Since $\mu_x = E(X)$, $\sigma_x^2 = E(X^2) - E^2(X)$, and similarly for Y, we may also write

$$\rho_{x,y} = \frac{E(XY) - E(X)E(Y)}{\sqrt{E(X^2) - E^2(X)}\sqrt{E(Y^2) - E^2(Y)}} \quad (3.5)$$

The correlation is 1 in the case of an increasing linear relationship, -1 in the case of a decreasing linear relationship, and some value in between in all other cases, indicating the degree of linear dependence between the variables. The closer the correlation is to either -1 or 1, the stronger the correlation between the variables. The correlation between the concurrent test results and the sequential test results are shown in Table 3.23.

Table 3.23 the cross-correlation coefficients of the sequential test and the concurrent test in harmonic shaking experiment.

Flow(cm/s)	7Hz	8Hz	9Hz
24	0.9872	0.9869	0.9776
25	0.9855	0.9754	0.9594
26	0.9925	0.9901	0.9835
27	0.9919	0.9893	0.9844
28	0.9949	0.9906	0.9863

Table 3.23 shows that the correlation between the scour result of sequential test and concurrent test increases as the shake frequency increases from 7 to 9 *Hz*, and the correlation also increases as the flow rate increases.

4. SCOUR WITH SIMULATED EARTHQUAKE EXPERIMENT

4.1 Experimental Setup:

The scour measurement device is upgraded after the harmonic shaking experiments. The laser sensor is mounted vertically over the sand bed instead of the angled configuration used earlier. Position measurement, therefore, can be made without adjustment for depth of the scour. This change resulted in faster measurements. The new scour depth measurement robot is shown in 4.1, 4.2.

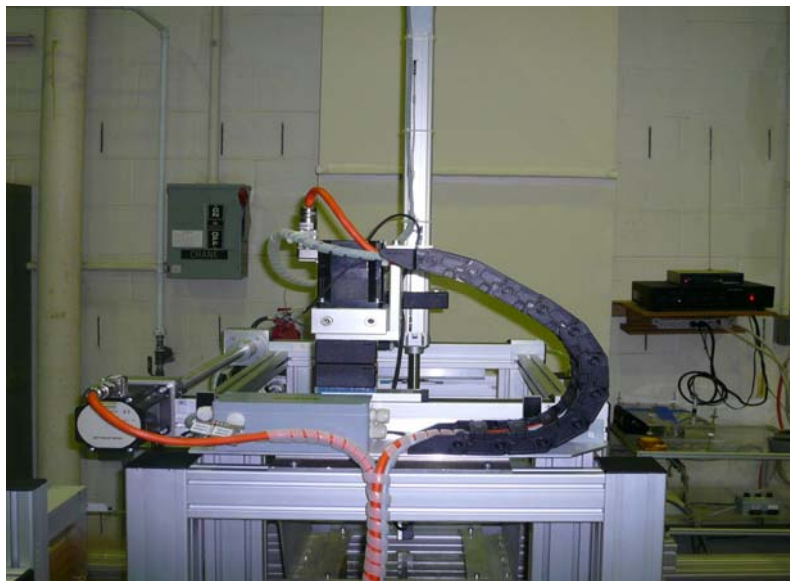


Figure 4.1 robot arm and positioning motor for the earthquake simulation test.



Figure 4.2 laser displacement sensor for the simulated earthquake shaking experiment.

The increased measurement speed allowed an increase of measurement points from 13 to 120 points, without sacrificing the time needed to make the measurements. The locations of the measured points of the new measurement robot are shown below.

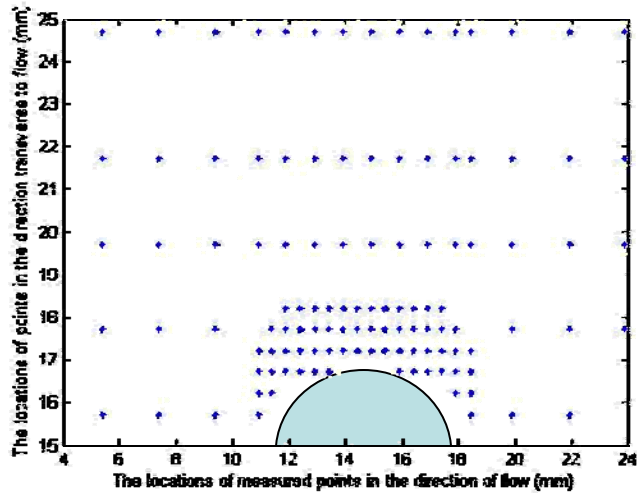


Figure 4.3 locations of measured points of the new measurement robot used in the simulated earthquake shaking experiment.

4.2 Experiment Procedures:

Chi Chi Earthquake record was used for this experiment. A high-velocity record was chosen as velocity is expected to influence scouring. The record was obtained from the PEER Strong Motion Database. It is designated as CHY101 N, recorded on 09/20/99. The record contains frequencies from 0.04Hz to 50Hz. The earthquake record has duration of approximately 8 seconds. The shaking is repeated for a total duration of 1 minute, so that the earthquake effect can be accentuated.

A Labview program was written to drive the linear motors to reproduce the earthquake motion. A screen capture of the Labview program is shown in

Figure 4.4 below:

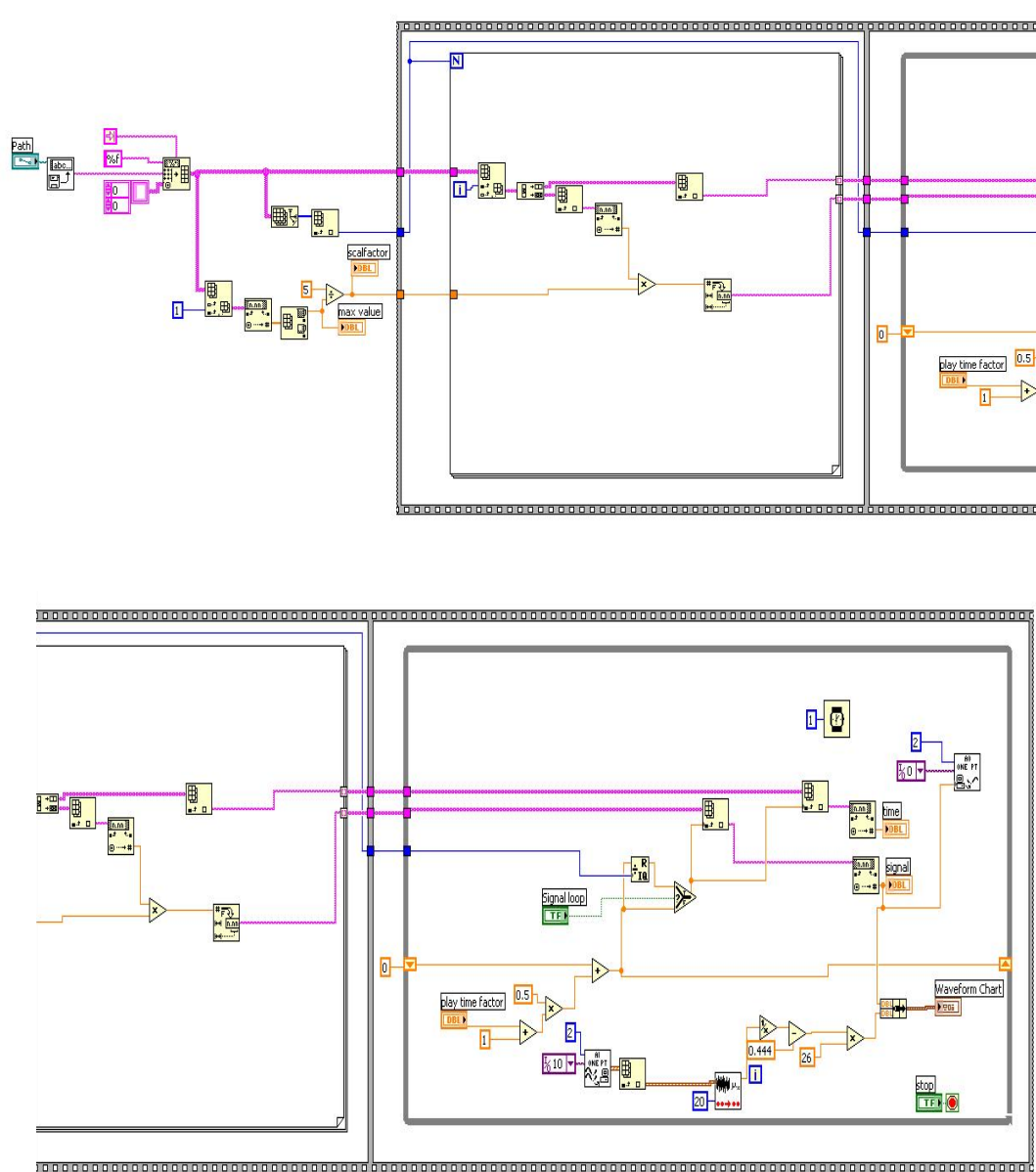


Figure 4.4 Labview program to simulate earthquake motions.

Figure 4.5 shows a time history of the earthquake displacements.

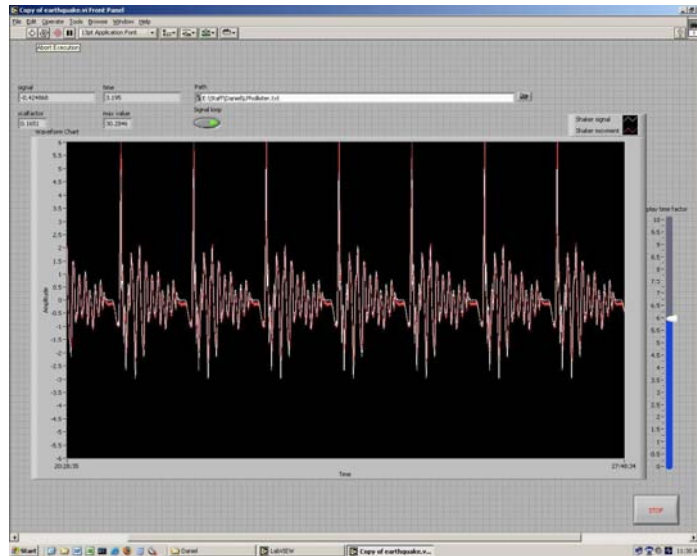


Figure 4.5 the frequencies of the simulated earthquake.

The white line in Figure 4.5 shows the input earthquake motion from the PEER database, and the red line shows the measured motion of the pier. The simulated motion is within less than 1 percent of the input displacement throughout the experiment.

The test protocols for the combined scouring and earthquake shaking experiment are as follows:

1. The sand surface is manually smoothed with a straight edge. The surface depths at predetermined coordinates are measured.
2. Scouring is performed at a specified flow rate for 1 minute. The surface depths at predetermined coordinates are measured.

3. Shaking with a simulate earthquake frequency for 1 minute. The surface depths at predetermined coordinates are measured.
4. Scouring at the specified flow rate again for 5 minutes. The surface depths at predetermined coordinates are measured.
5. The sand surface is manually smoothed with a straight edge again. The surface depths at the predetermined coordinates are measured.
6. Scouring and shaking at specified flow rate and simulate earthquake frequency are performed simultaneously for 1 minute, and then the surface depths at the predetermined coordinates are measured.
7. After the initial tests at 25 cm/s and 26 cm/s , it was decided to allow the flow to continue after the final earthquake motion. Therefore an additional step was added to the tests with 27 and 28 cm/s flow. Scouring at the specified flow rate again for 5 minutes. The surface depths at predetermined coordinates are measured.

The reason for adding this step into the experiment is that earthquake is a short-term event. Step 7 is used to measure the effect of scour after the earthquake shaking to observe any lasting effect of earthquake on scouring.

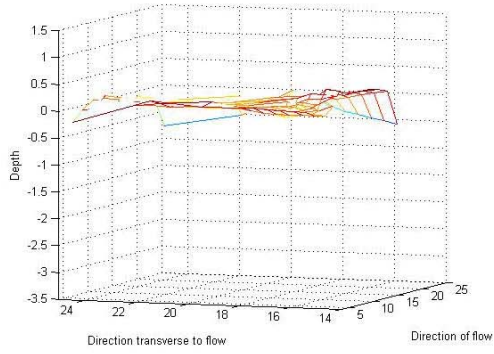
For the harmonic shaking experiment, we applied the flow rates from 24 cm/s to 28 cm/s . However, results indicated that 24 cm/s flow rate was insufficient to

cause significant scouring. Therefore, we only conducted the tests with flow rates from 25 *cm/s* to 28 *cm/s* for the study of scour and simulated earthquake shaking.

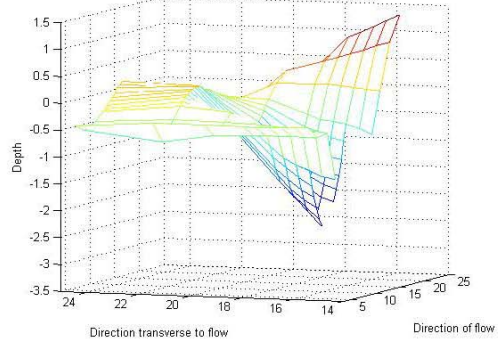
4.3 Results Observations:

The surface after each step of the experiment is measured using the laser measurement robot. Due to the increase of measurement points in this set of experiment, the scoured surfaces can be shown by three dimensional plots with enough measurement points. These plots are shown in Figures 4.6 to 4.9.

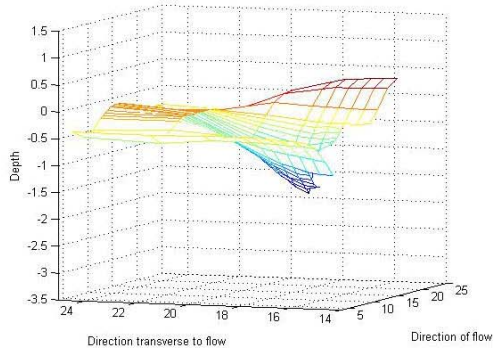
1st test- flating the sand



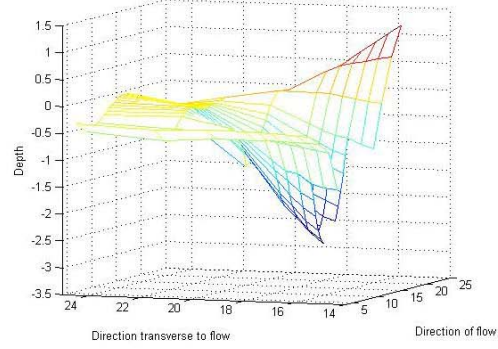
2nd test- scouring for 5 minutes



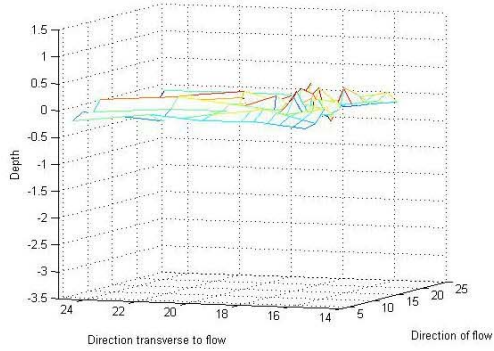
3rd test- shaking for 1 minurw



4th test- scouring for 5 minutes



5th test- reflating the sand



6th test- scouring and shaking for 1 minute

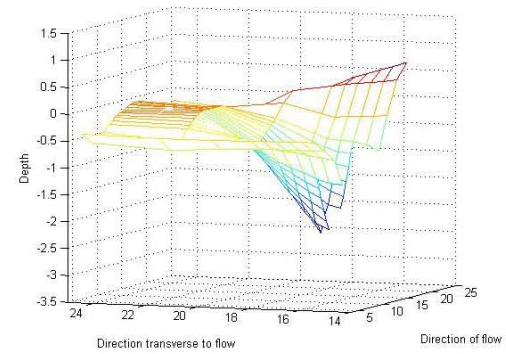
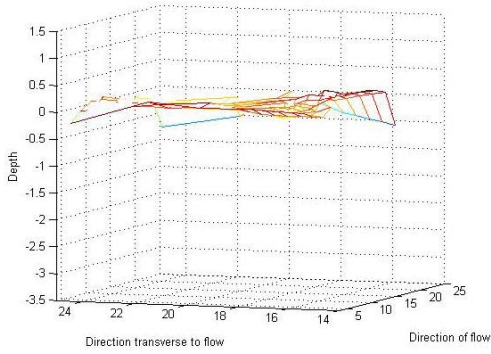
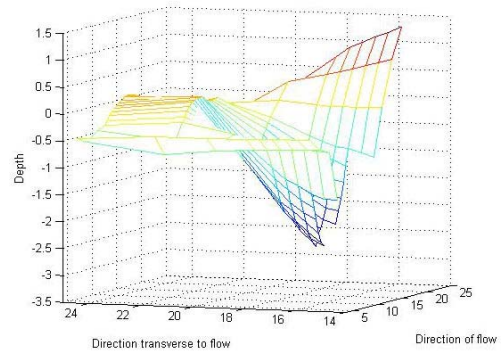


Figure 4.6 Mesh plot of scoured surface for 25cm/s flow rate test.

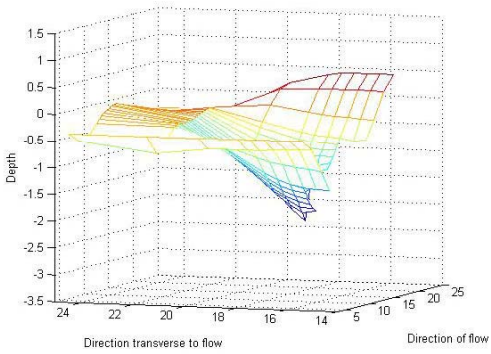
1st test- flating the sand



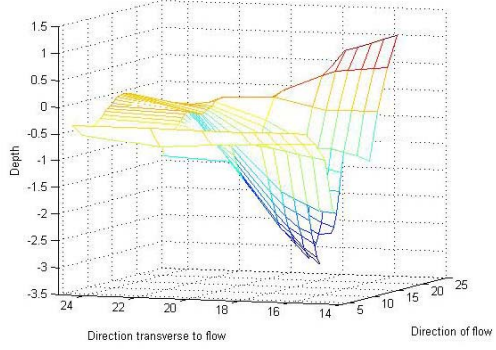
2nd test- scouring for 5 minutes



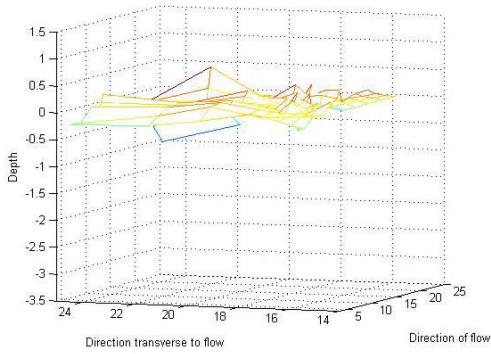
3rd test- shaking for 1 minute-



4th test- scouring for 5 minutes



5th test- reflatting the sand



6th test- scouring for 5 minutes

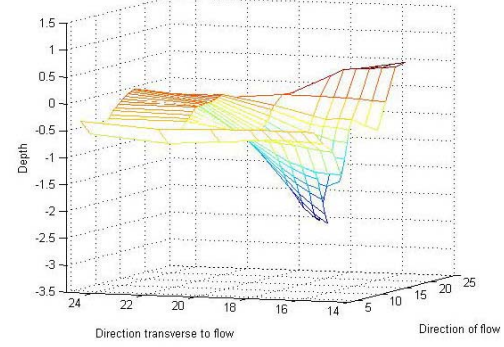
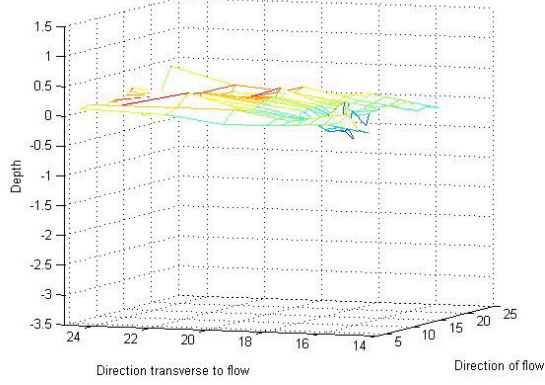
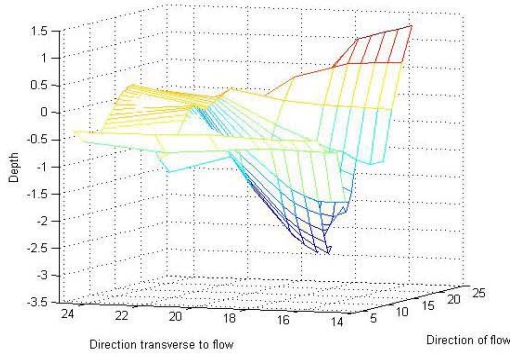


Figure 4.7 Mesh plot of scoured surface for 26cm/s flow rate test.

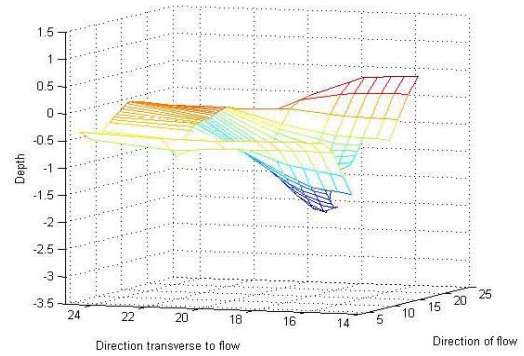
1st test- flating the sand



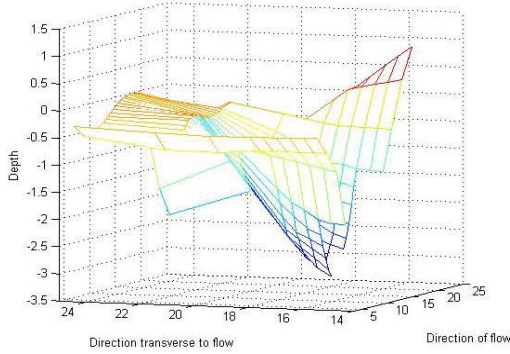
2nd test- scouring for 1 minute



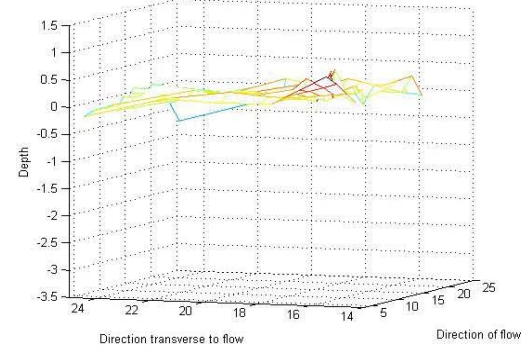
3rd test- shaking for 1 minute



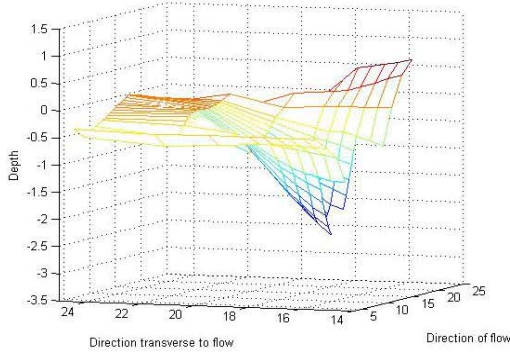
4th test- scouring for 5 minutes



5th test- reflat the sand



6th test- scouring and shaking



7th test- scouring for 5 min-

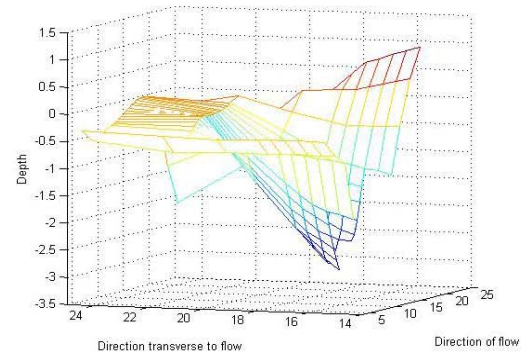
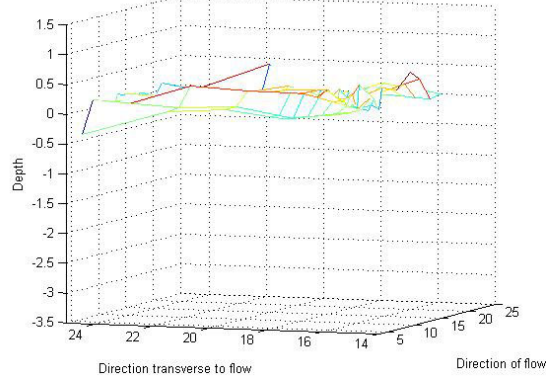
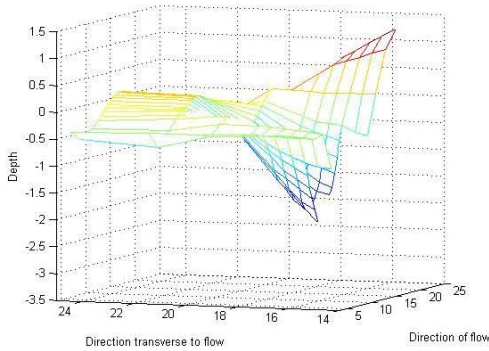


Figure 4.8 Mesh plot of scoured surface for 27cm/s flow rate test.

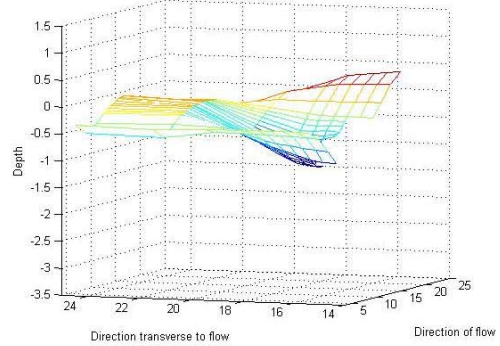
1st test- flating the sand



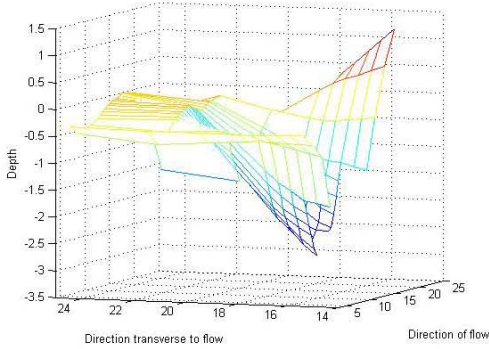
2nd test- scouring for 1 minute



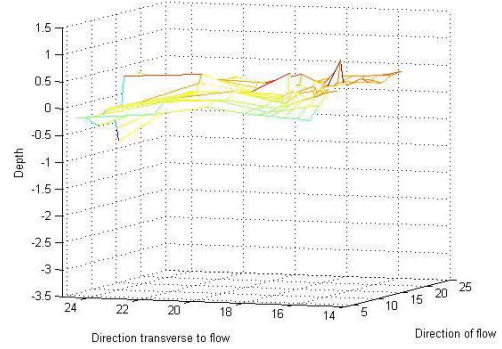
3rd test- shaking for 1 minute



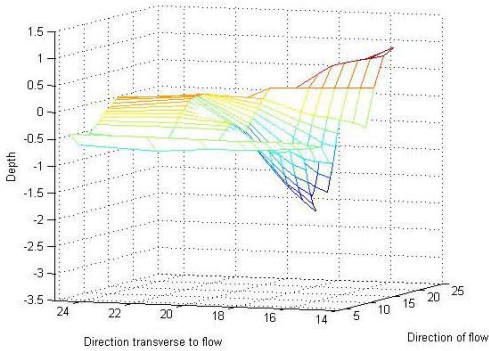
4th test- scouring for 5 minutes



5th test- reflating the sand



6th test- scouring and shaking for 1 minute



7th test- scouring for 5 minutes

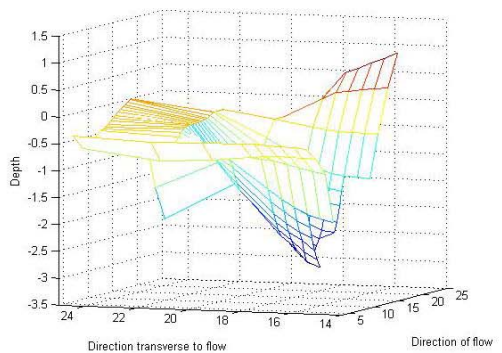
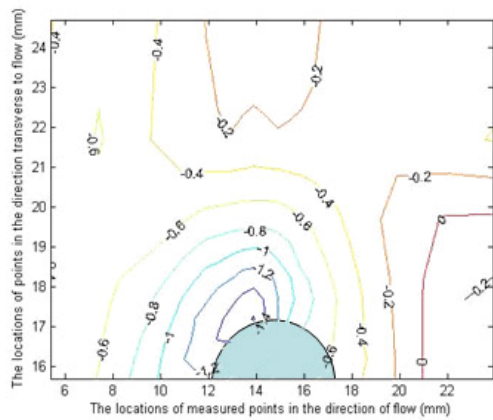
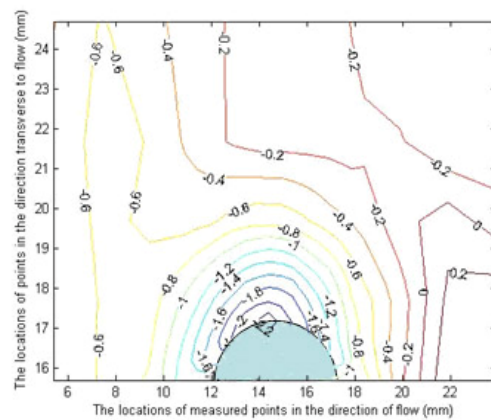


Figure 4.9 Mesh plot of scoured surface for 28cm/s flow rate test.

While the three dimensional plots are easy to understand, comparisons of the surfaces using a single point of view are rather difficult. To facilitate comparison of the surface when the scour and earthquake motions are imposed sequentially or concurrently, two dimensional contour plots are used. Figure 4.10 to 4.15 show comparisons of the contour surfaces at different flow velocities. The figures on the left are the surface contour if the stream bed is allowed to scour for 1 minute, and then it is followed by a 1 minute earthquake motion. The figures on the right represent surface contours if scouring and earthquake motions occur simultaneously.

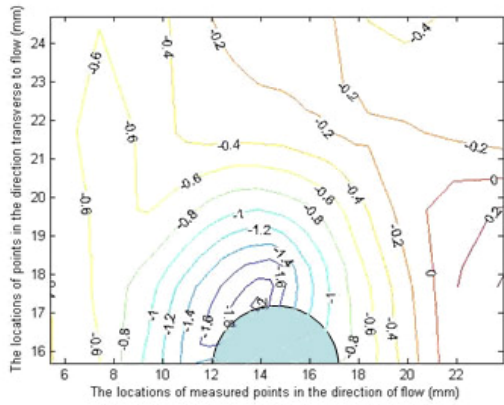


(a)

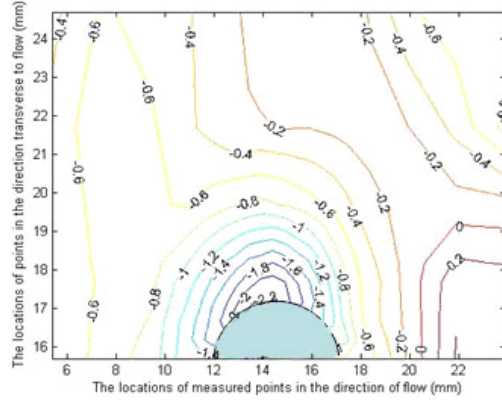


(b)

Figure 4.10(a) the contour plot of the sequential test with 25cm/s flow rate.
 (b) the contour plot of the concurrent test with 25cm/s flow rate.

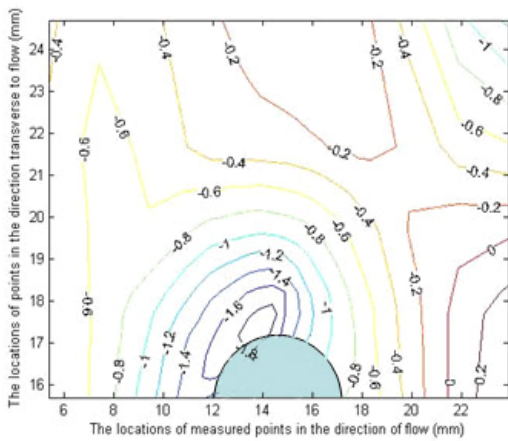


(a)

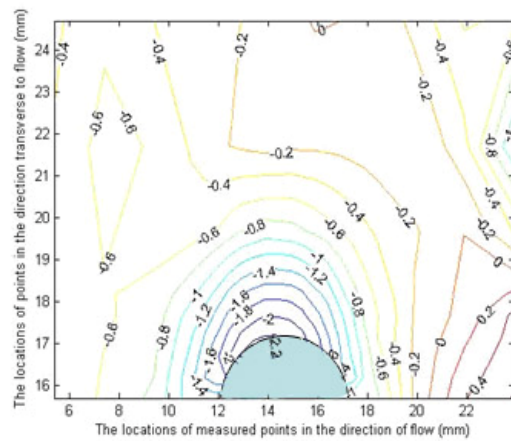


(b)

Figure 4.11(a) the contour plot of the sequential test with 26cm/s flow rate.
 (b) the contour plot of the concurrent test with 26cm/s flow rate.

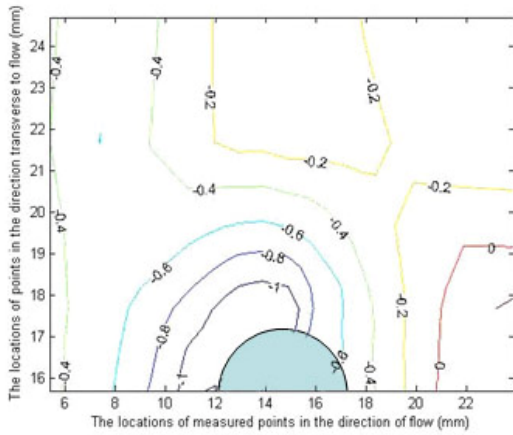


(a)

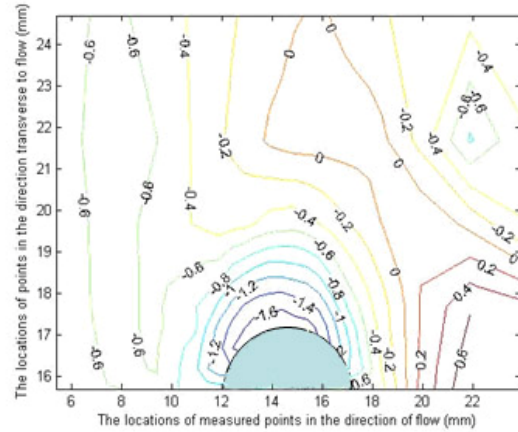


(b)

Figure 4.12(a) the contour plot of the sequential test with 27cm/s flow rate.
 (b) the contour plot of the concurrent test with 27cm/s flow rate.

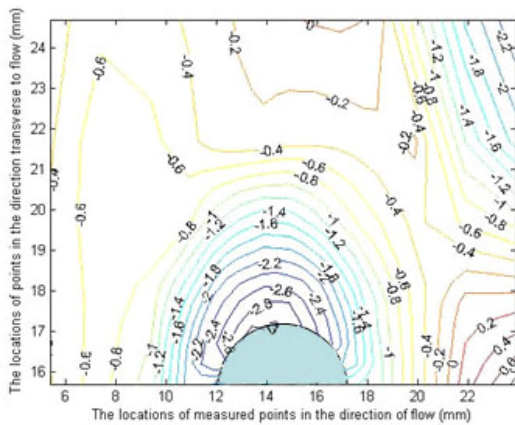


(a)

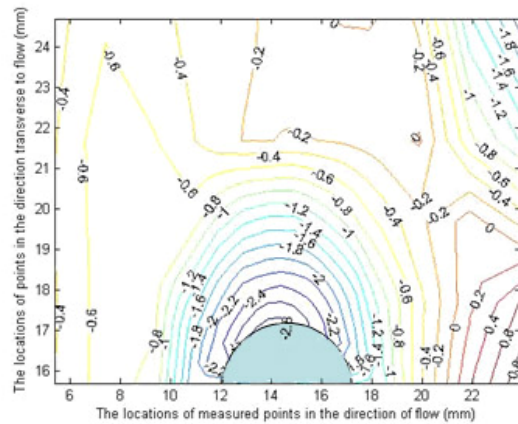


(b)

Figure 4.13(a) the contour plot of the sequential test with 28cm/s flow rate. (b) the contour plot of the concurrent test with 28cm/s flow rate.



(a)



(b)

Figure 4.14(a) the contour plot of the scouring after sequential test with 27cm/s flow rate. (b) the contour plot of the scouring after concurrent test with 27cm/s flow rate.

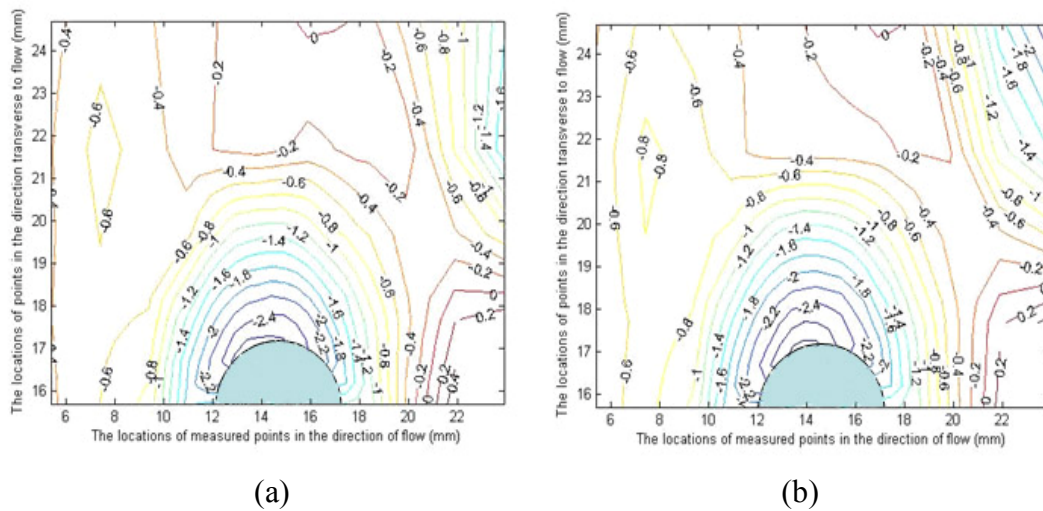


Figure 4.15(a) the contour plot of the scouring after sequential test with 28cm/s flow rate. (b) the contour plot of the scouring after concurrent test with 28cm/s flow rate.

4.4 Result Discussion:

The experiments are repeated with simulated earthquake motion. As described before, surface measurements were changed to include more points. Again, the results after scouring and shaking independently are superimposed in Test 3, then the results compared to the scoured surface if scouring and shaking are tested concurrently in Test 6.

Since earthquakes are short-term events and scouring are long-term events. It seems likely that the effect of earthquake would not make a difference on the long term effects of scouring. One way to verify this hypothesis is to allow the scour to continue after the tests with scour and shaking were performed concurrently and sequentially. In other words, the comparisons are for Test 4: 1

minute of scour, followed by 1 minute of earthquake shaking, then 5 minutes of scouring, and Test 7: 1 minute of scouring and shaking concurrently, followed by 5 minutes of scouring. Tests 4 and 7 are done at the flow rates of 27cm/s and 28cm/s only. As in Section 5.1, maximum depth, root mean square and correlation of the results between Test 4 and Test 7 are made.

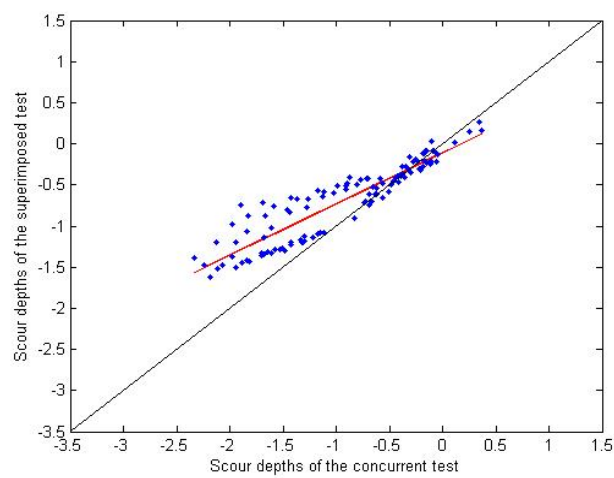


Figure 4.16 Scatter plot of the scour depths of the sequential test versus concurrent test with flow rate of 25cm/s for the simulated earthquake experiment.

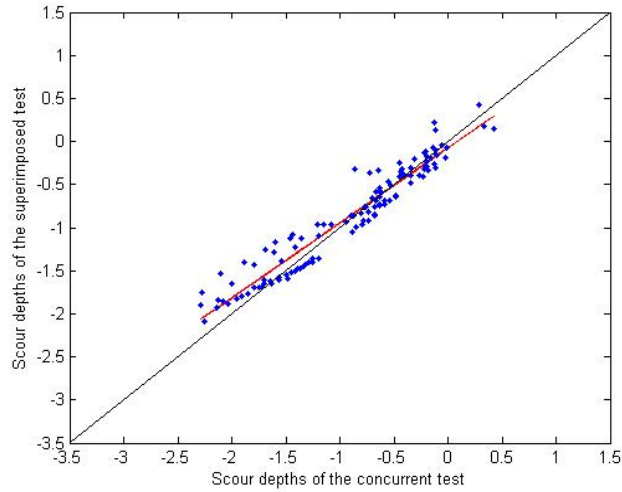


Figure 4.17 Scatter plot of the scour depths of the sequential test versus concurrent test with flow rate of 26cm/s for the simulated earthquake experiment.

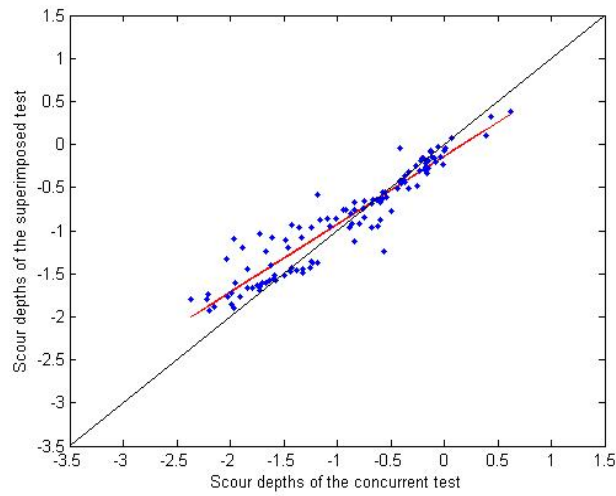


Figure 4.18 Scatter plot of the scour depths of the sequential test versus concurrent test with flow rate of 27cm/s for the simulated earthquake experiment.

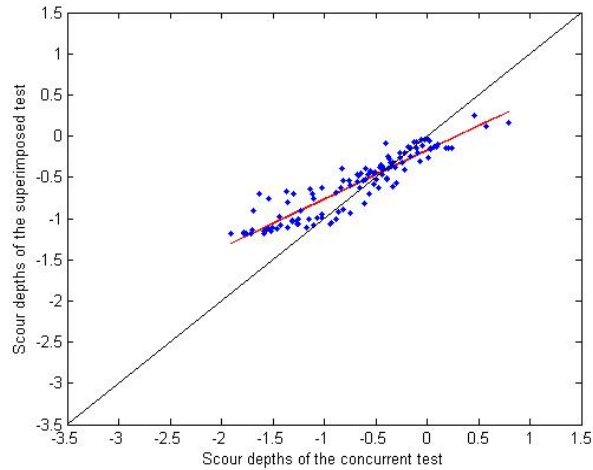


Figure 4.19 Scatter plot of the scour depths of the sequential test versus concurrent test with flow rate of 28cm/s for the simulated earthquake experiment.

Figures 4.16 to 4.19 show that in general the sequential tests generate mounds that are lower, and holes that are shallower. This result is expected, but compared to the shaking at a constant frequency, the difference between the sequential tests and the concurrent tests are smaller when a spectrum of frequencies is used. While the depths at some points from the scour after sequential test (fourth test) and scour after concurrent test (seventh tests) are very different. Linear regression shows that the overall difference between them is very small.

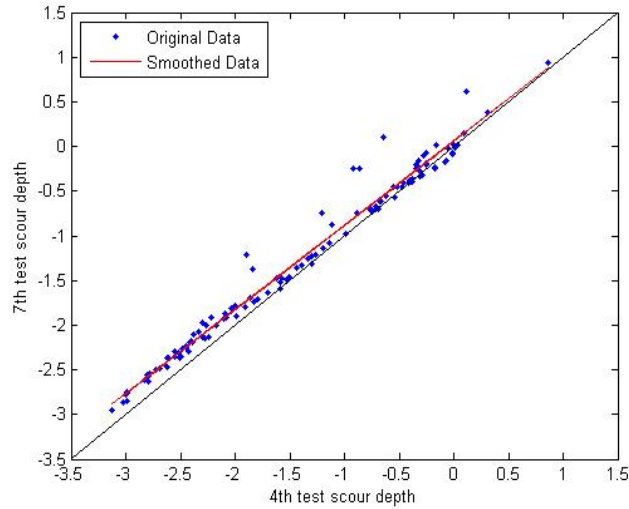


Figure 4.20 Scatter plot of the scour depths of the sequential test after scouring versus concurrent test after scouring with flow rate of 27cm/s for the simulated earthquake experiment.

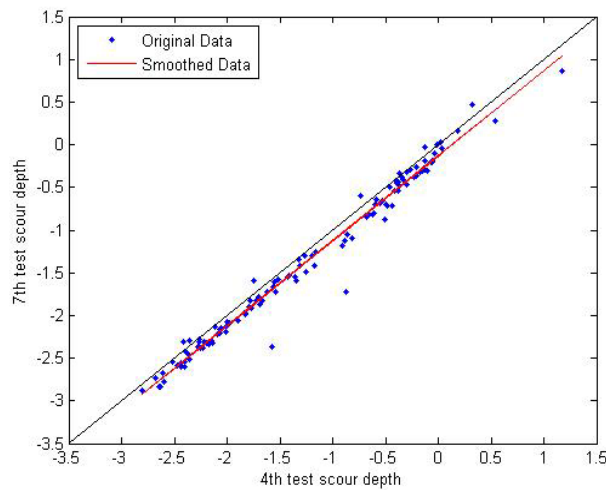


Figure 4.21 Scatter plot of the scour depths of the sequential test after scouring versus concurrent test after scouring with flow rate of 28cm/s for the simulated earthquake experiment.

The root mean squares of the differences between sequential and concurrent test results calculated by Equation 3.1 are compared in Table 4.1, and the comparison of scour after sequential test and scour after concurrent test are shown in table 4.2.

Table 4.1 the root mean squares of the differences between sequential tests and concurrent tests.

Flow Rate	25 cm/s	26 cm/s	27 cm/s	28 cm/s
RMS	0.035	0.017	0.022	0.056

Table 4.2 the root mean squares of the differences between scour after sequential tests and scour after concurrent tests.

Flow Rate	27 cm/s	28cm/s
RMS	0.019	0.016

By comparing Table 4.1 to Table 3.18, it is observed that when a spectrum of frequencies is applied, the differences between sequential tests and concurrent tests are smaller than the tests in which a constant frequency is applied.

At the flow rates of 27 cm/s and 28 cm/s, scouring was continued after the shaking motions were applied. Table 4.2 shows that the difference between sequential test and concurrent test, after additional scouring, is comparatively small.

The percent difference between the maximum scour depths for the sequential tests and the concurrent tests are compared in Table 4.3.

Table 4.3 the percent errors of the maximum scour depths of sequential tests vs. concurrent tests.

Flow Rates	25cm/s	26cm/s	27cm/s	28cm/s
Percent Errors	30.776%	8.432%	18.562%	37.729%

The maximum scour depths after additional scouring are compared in Table 4.3. As for the overall difference between these tests, the difference between the maxima is also very small. It should be noted that maxima of transient quantities such as stresses and deformations may be important to the strength and durability of the structure, but they were not within the scope of the experiments performed.

Table 4.4 the percent difference of the maximum scour depths of scouring after sequential tests vs. scouring after concurrent tests.

Flow Rates	27cm/s	28cm/s
Percent Errors	5.832%	2.844%

Cross-correlation coefficients of the data from the sequential and the concurrent tests give a measure of the amount of scatter in the data. Figures 4.16 to 4.19 show that the results are highly correlated. Table 4.5 shows that the results of sequential tests are highly correlated with the results of concurrent tests.

Table 4.5 the cross-correlation coefficients of the sequential tests versus the concurrent tests in different flow rates.

Flow rate(cm/s)	The CC. of the 3 rd tests vs. the 6 th tests
25	0.9267
26	0.9664
27	0.9481
28	0.9266

As can be observed in Figures 4.20 and 4.21, Table 4.6 shows that the cross correlation between the 4th and 7th tests is close to 1.

Table 4.6 the cross-correlation coefficients of the scouring after sequential tests versus the scouring after concurrent tests with different flow rates.

Flow rate (cm/s)	The CC. of the 4th vs. the 7th test
27cm/s	0.9901
28cm/s	0.9907

6. CONCLUSION

Bridge structures are often subjected to multiple hazards, for example, scouring of the foundation from water flow and shaking induced by earthquake or vehicle impact. Predicting the effects of multiple hazards is difficult as analytical tools for their combined effects are seldom available. Often, the best that can be done is to consider each hazard as an individual event that occurs sequentially. In the event of the combined actions of scouring and earthquake shaking, it may be reasonable to study the effects of scouring, and then add the effects of the shaking after the effects of scouring have been obtained.

The hypothesis in the present work is that the combined effects of scouring and shaking of a bridge pier is different from the addition of the effects of scouring followed by shaking. This is theorized as the individual effect is nonlinear in nature. We expect the shaking could undo some of the effects of scouring. This is especially true if scouring precedes shaking. However, when these events occur concurrently, the results of canceling effect of shaking on scouring is expected to be smaller. A shaking flume designed to verify this theory was designed and built at Turner-Fairbank Highway Research Center (TFHRC) of the Federal Highway Research Administration (FHWA).

The water depth of the shaking flume was kept constant at 8 cm . The

experiments were divided into two parts: one for scouring and harmonic shaking, which simulated continuous vibrations such as traffic-induced motion. Experiments were performed at the flow rates from 24 cm/s to 28 cm/s (critical velocity for sediment transport) and shaking frequencies of 7, 8, and 9 Hz . The second part of the experiments combined scouring and earthquake shaking. Earthquake displacement record from the Chi Chi earthquake, taken from a station where the peak velocity was particularly high, was applied to the shaking flume. Flow rates from 25 cm/s to 28 cm/s were used for the first set of experiments that combined simulated earthquake shaking. A single pier with a round cross section was used for the experiment.

To verify the hypothesis, experimental results of the combined effects of shaking and scouring (Data set 6) are compared to the effects of scouring followed by shaking (Data set 3). Scatter plots of depths of scoured holes of Data set 3 are compared to the depths from Data set 6. Variables for comparison included maximum depth and total volume. Based on the experimental data obtained in the experiments described above, the following conclusions can be made:

1. The scour depth of the combined shaking and scouring experiment is different from the scour depth of the experiments where shaking and

scouring are performed independently. The difference of the scour depths for these tests range from 0.3% to 145%.

2. The differences of the scour results for the sequential tests and the concurrent tests are dependent on the shaking frequency for the harmonic shaking experiment. For the 7 Hz test, the percent difference of the maximum scour depths between concurrent and sequential test varied from 0.30 % to 11 %. At 9 Hz, the percent difference of the maximum scour depths between concurrent and sequential test varied from 45%% to 145%.
3. Performing the scouring and shaking sequentially has the effect of flattening the mounds and filling the scoured holes. However, this effect is smaller when the scouring and shaking are performed concurrently.
4. When frequencies content is broader (from an earthquake record), the correlation of the sequential tests and the concurrent tests are smaller than those where a single frequency is used. The correlation coefficients of the different test methods range from 0.93 to 0.97, when frequency content varied from 0.04Hz to 50Hz. When a sinusoidal shaking at 7, 8, or 9 Hz was used, the correlation coefficients ranged from 0.96 to 0.99.

5. When additional scouring is allowed after the shaking motion is applied, the final scouring effect is similar whether the shaking was performed concurrently with scouring or sequentially. Cross-correlation coefficient between the scour depths of concurrent test and sequential test varied from 0.9901 to 0.9907 as the flow rate changed from 27 *cm/s* to 28 *cm/s*.

The experiments represent a preliminary test to show the possibility of synergy between shaking and scouring. Future works should include stresses and deformation of the structure during the combined event of scouring and earthquake motion, as short-term but high-level forces may have a significant effect on the safety of the structure. It should be pointed out that the current experiments are performed with the top of the pier fixed. This fixity kept the pier from displacing or rotating relative to the foundation, but a bridge pier may have relative displacement or rotation to the foundation during shaking, and the rocking motion is likely to increase the effect of scouring. Therefore, future tests should be designed to allow some relative motion at the top of the pier.

7. REFERENCE

1. Office of bridge development manual on hydrologic and hydraulic design (2007), "Chapter 11 evaluating scour at bridges, Fourth Edition". Publication No. FHWA NHI 01-001, Hydraulic Engineering Circular No. 18.
2. Melville, B. W., and Sutherland, A.J. (1988) "Design method for local scour at bridge piers" *J. Hyd. Eng., ASCE*, Vol. 114, HY10, pp. 1210-1226.
3. Bruce W. Melville, Stephen E. Coleman (2000). "Bridge Scour". Technology & Engineering, ISBN 1887201181.
4. Abdul Karim Barbhuiya, Subhasish Dey (2004). "Local scour at abutments: A review" [online]. Available: <http://www.ias.ac.in/sadhana/Pdf2004Oct/Pe1183.pdf> [accessed 03 April 2008].
5. Chin-Lien Yen, Jihn-Sung Lai, and Wen-Yi Chang (2000) "Modeling of 3D Flow and Scouring around Circular Piers", *Proc. Natl. Sci. Counc. ROC(A)* Vol. 25, No. 1, 2001. pp. 17-26.
6. Vasileios G. Matziaris, (2004). Slope stability and earthquake-induced displacement analysis in GIS Environment [online]. Available: http://users.ntua.gr/vmatziar/MSc_Dissertation.pdf [accessed 14 February, 2008].

7. Alan F. Rauch (1997). "EPOLLS: An Empirical Methods for Predicting surface Displacements Due to Liquefaction-Induced Lateral Spreading in Earthquake" [Online]. Available:

<http://scholar.lib.vt.edu/theses/available/etd-219182249741411> [accessed 23 April, 2008].

8. Randall W. Jibson, (1993), "Predicting Earthquake-Induced Landslide Displacements Using Newmark's Sliding Block Analysis", Transportation Research Record No. 1411, pp. 9-17.

9. Ambraseys N., Srbulov M. (1995). "Earthquake induced displacements of slopes" International Journal of Rock Mechanics and Mining Sciences and Geomechanics Abstracts, Volume 33, Number 1, January 1996 , pp. 35A-35A(1).

10. M. Muzzammil, T. Gangadhariah (2003). "The Mean Characteristics of Horseshoe Vortex at a Cylindrical Pier". Journal of Hydraulic Research, Vol. 41, No. 3 (2003), pp. 285–297.

11. Peter C. Chang, PhD, Miguel A. Gonzalez, (2006). "Pier scours in simulated earthquake in laboratory flume. [Online]". Available:

http://www.isr.umd.edu/research/REU_reports/2005_PPTs/Gonzalez.doc

[accessed 12 December, 2007]

12. Veronica M. Ghelardi, (2004). "Estimation of long term bridge pier scour in cohesive soils at Maryland bridges using EFA/SRICOS" [online]. Available: <https://drum.umd.edu/dspace/bitstream/1903/1816/1/umi-umd-1801.pdf> [accessed 12 October, 2007].
13. Chiew, Y. M., and Melville, B.W. (1987) "Local scour around bridge piers" *Journal of Hydraulic Research*, Vol. 25, No. 1, pp. 15-26.
14. Breusers, H. N. C., Nicollet, G. and Shen, H. W. (1977) "Local scour around cylindrical piers" *Journal of Hydraulic Research*, Vol. 15, No. 3, pp 211-252.
15. Babaeyan-Koopaei K., and Valentine, E. M. (1999) "Bridge pier scour in self-formed laboratory channels". The XXVIII IAHR congress, pp22-27.